The high-light-tolerant desert alga *Chlorella ohadii* is protected from oxidative stress by a non-photochemical quenching-independent mechanism

Guy Levin[1]*,**, Michael Yasmin[1]*, Oded Liran[2], Rawad Hanna[1], Oded Kleifeld[1], Guy Horev[3], Francis-André Wollman[4], Wojciech J. Nawrocki[4] and Gadi Schuster[1,5]**

[1] Faculty of Biology, Technion, Haifa, 32000 Israel

[2] Kineret Limnological Laboratory, Horvat Kur, 1495000 Israel

[3] Migal Galilee Research Institute Ltd, Qiryat Shemona, 11016 Israel

[4] Unité Mixte de Recherche 7141, Centre National de la Recherche Scientifique, Sorbonne Université, Institut de Biologie Physico-Chimique, Paris, France

[5] Grand Technion Energy Program, Technion, Haifa, 32000 Israel

*These authors have equally contributed to this work

**Corresponding authors: guylevin@campus.technion.ac.il or guylevin5@gmail.com (GL), gadis@technion.ac.il (GS)

Contact (for submission purposes): guylevin@campus.technion.ac.il

Running title: NPQ-independent photoprotection in a desert alga

Abstract

Non-photochemical quenching (NPQ) mechanisms are crucial for protecting photosynthesis from photoinhibition in plants, algae, and cyanobacteria, and their modulation is a long-standing goal for improving photosynthesis and crop yields. The current work demonstrates that *Chlorella ohadii*, a green micro-alga that thrives in the desert under high light intensities which are fatal to many photosynthetic organisms, does not perform nor require NPQ to protect photosynthesis under constant high light. Instead of dissipating excess energy, it minimizes its uptake by eliminating the photosynthetic antenna of photosystem II, in addition to accumulating antioxidants that neutralize harmful reactive oxygen species (ROS) and ramping up cyclic electron flow around PSI. This NPQ-independent response proved efficient in preventing ROS accumulation and reducing oxidative damage to proteins in high-light-grown cells. This work contributes to the understanding of photoprotection under extreme high light intensities and provides potential targets for improving photoprotection.

Introduction

Light drives photosynthesis, but also damages the photosynthetic apparatus in several ways. Particularly, illumination facilitates the generation of reactive oxygen species (ROS) which damage the molecular players in photosynthesis, thereby inhibiting the process – an effect known as photoinhibition (Ögren, 1988; Ögren and Sjöström, 1990). Under high light (HL) conditions regulated non-photochemical quenching (NPQ) mechanisms through which excess absorbed light energy is harmlessly dissipated as heat, are considered crucial for photosynthesis protection (photoprotection) (Delosme, 1967; Wolff and Witt, 1969; Demmig-Adams et al., 1989; Demmig-Adams et al., 1990). q_E quenching, the major NPQ component, is located within the membrane-intrinsic major photosystem II (PSII) light-harvesting complex (LHCII) and is activated by the trans-thylakoid ΔpH gradient that forms as the result of photosynthetic electron transport. Typically, q_E is the strongest and the most rapidly triggered component of NPQ in the green lineage, undergoing activation in seconds, as recently reviewed by (Bassi and Dall'Osto, 2021). During periods of high photosynthetic activity, the thylakoid lumen is acidified due to proton translocation across the thylakoid membrane by the combined activity of linear and cyclic photosynthetic electron flows (LEF and CEF). PsbS and LhcSR in plants and algae, respectively, act as proton sensors and upon acidification of the lumen, induce qE to dissipate excess energy as heat (Li et al., 2000; Li et al., 2004; Peers et al., 2009; Liguori et al.,

2013). Simultaneously, the xanthophyll cycle is activated, and newly formed zeaxanthin interacting in the PSII-LHCII chlorophyll pool provides pathways for energy dissipation. (Demmig et al., 1987; Niyogi et al., 1998; Xu et al., 2015; Sacharz et al., 2017).

Chlorella ohadii is a green micro-alga that thrives in the desert, where it is exposed to extremely high light intensities (Treves et al., 2013; Levin et al., 2021). Accordingly, *C. ohadii* is highly tolerant to photoinhibition (Treves et al., 2016; Levin et al., 2023; Levin et al., 2024). It has been found that the adaptation of *C. ohadii* to HL involves marked changes in the thylakoids of which the most pronounced are the large size reductions in the PSII antenna, the LHCII, as well as the massive accumulation of carotenoids and several photoprotective proteins (Levin et al 2021, 2023). HL-grown *C. ohadii* does not undergo state transitions, a mechanism of antenna exchange between PSII and PSI (Bonaventura and Myers, 1969; Chow et al., 1981; Delosme et al., 1996), considered to be photoprotective (Allorent et al., 2013; Nawrocki et al., 2016). Moreover, *C. ohadii* lacks LhcSR in its genome and does not accumulate the PsbS protein (Treves et al., 2016; Levin et al., 2023; Murik et al., 2024), suggesting the absence of q_E. Interestingly, carotenoid biosynthesis-related protein (CBR), which belongs to the LHC-like protein family with a structure similar to PsbS, accumulates to a great extent in HL-grown *C. ohadii* (Levy et al., 1993; Levin and Schuster, 2023; Levin et al., 2023). Structural modeling suggested that one of the proton-sensing glutamates of PsbS was conserved in CBR, raising the possibility of its role in lumen acidification sensing. Moreover, fractionation of the photosynthetic protein complexes by sucrose density gradient centrifugation showed that CBR from HL-grown cells co-localized with a detached fraction of LHCII and carotenoids, both of which are associated with NPQ and ROS scavenging (Levin et al., 2023). However, it was observed that the HL-grown *C. ohadii* eliminates most of the LHCII, resulting in a major reduction of light absorption by PSII (Levin et al., 2021; Levin et al., 2023). Given that the LHCII is the major site of NPQ (Ruban et al., 1999; Elrad et al., 2002; Sacharz et al., 2017; Nicol and Croce, 2021), its elimination and the lack of LhcSR raise functional questions about the mode of photoprotection in *C. ohadii*.

The current work investigated the role and interplay of the elimination of the PSII antenna, NPQ, and CEF on ROS accumulation and oxidative damage in *C. ohadii*. The analysis found that q_E is absent and replaced with an NPQ-independent mechanism in HL-grown *C. ohadii* cells. This mechanism mainly relies on LHCII elimination and the consequent enhancement of CEF around PSI. Additionally, the high accumulation of CBR, carotenoids, and other antioxidants indicates that *C. ohadii*, adapted to grow at extremely high light intensity, employs both active and passive mechanisms of photoinhibition resistance. These adaptations lead to

reduced production and low accumulation of harmful ROS in response to HL, resulting in limited oxidative damage to proteins in HL-grown cells. The work demonstrates that NPQ is not required to withstand excess illumination in HL-grown *C. ohadii* and that under conditions of prolonged exposure to HL intensities, minimizing the PSII-LHCII absorption cross-section and ROS production while maximizing antioxidant activity has been selected as the most successful strategy to avoid photoinhibition.

Results

HL-grown cells upregulate CBR and enzymatic antioxidant expression and accumulate less oxidative damage. To understand the extraordinary resistance of *C. ohadii* to HL intensities, the strain was grown under low and high light conditions (LL: 50 µmol photons m^{-2} s^{-1}; HL: 2000 µmol photons m^{-2} s^{-1}), and then subjected to label-free quantification mass spectrometry (LFQ-MS) to detect possible enzymatic antioxidants that participate in the detoxification of ROS and determine their effect on chloroplast protein oxidation. As was observed for isolated thylakoid membranes (Levin et al., 2023), CBR was the most accumulated protein in HL-grown cells, with a 995-fold change compared to LL-grown cells. This was accompanied by a drastic loss of LHCII subunits in HL-grown cells (Figure 1A). The LHCI abundance change was much smaller than the LHCII downregulation, indicating that PSII function was the most affected. Additionally, 15 enzymes known to participate in ROS detoxification or to contribute to energy dissipation via electron extraction from the photosynthetic electron transport chain, were identified (Figures 1A and 1B). Specifically, two isoforms of superoxide dismutase (SOD), which catalyzes the detoxification of superoxide (O_2^-) by converting it to H_2O_2, were detected, one of which was statistically significantly accumulated in HL-grown cells (1.8-fold higher compared to LL-grown cells). Of glutathione peroxidase (GPX) and ascorbate peroxidase (APX), which can further detoxify H_2O_2 by catalyzing its conversion to water (H_2O), only GPX was significantly accumulated in the HL-grown cells (3.3-fold change). Dehydroascorbate reductase (DHAR) and two isoforms of glutathione-s-transferase (GST), enzymes that participate in the detoxifying ascorbate-glutathione cycle, were also significantly accumulated in HL-grown cells (3.8-, 1.9- and 1.2-fold change, respectively). No statistically significant changes in HL-grown cells were measured for catalase, which catalyzes the conversion of H_2O_2 to H_2O (1.3-fold change). ω-3 fatty acid desaturase (ω3FAD), which catalyzes the generation of polyunsaturated fatty acids (PUFAs), underwent 2.1-fold accumulation in HL- compared to LL-grown cells. PUFAs have been suggested to contribute to ROS detoxification by interacting with ROS during lipid peroxidation (Schmid-Siegert et al., 2016). Flavodiiron proteins (Flv1

and Flv2) which are proposed electron sinks possibly involved in PSII and/or PSI photoprotection (Burlacot et al., 2022; Bag et al., 2023; Calzadilla et al., 2024), were significantly accumulated in HL-grown cells (2.9- and 8.4-fold change, respectively), providing an additional route for energy dissipation. In contrast, PTOX, another putative electron sink, was not differentially accumulated in HL-grown cells (0.9-fold change) (Figure 1A and 1B).

Intensity-based absolute quantification (iBAQ) (Schwanhäusser et al., 2011) was then used to determine which of the accumulated enzymes were highly abundant in HL-grown *C. ohadii* cells and thus likely to be important for photoprotection (Figure 1B). Out of the abovementioned enzymes, SOD was the most abundant protein in HL-grown cells (top 0.7% percentile compared to all detected proteins), followed by GPX (6.7%) and CBR (7.9%). (Figure 1B). This further highlights the probable importance of CBR and specifically known enzymatic antioxidants for photoprotection. Other enzymes were either less abundant or not accumulated in HL-grown cells compared to LL-grown cells.

The extent of oxidative damage was then assessed by quantifying the irreversible oxidation of tryptophan, which leads to protein degradation (Kato et al., 2023). Remarkably, Oxidized peptides of PSII, LHCII, PSI, and LHCI subunits, alongside most other detected oxidized peptides of many different proteins, were majorly accumulated in LL-grown cells when compared to HL-grown cells (Figure 1C). This remarkable difference between LL- and HL-grown cells indicates the high efficiency of ROS scavenging in HL-grown cells. The proteomics analysis suggested that in addition to the robust downregulation of LHCII and marked accumulation of carotenoid in HL-grown cells (Levin et al., 2021; Levin et al., 2023), SOD and GPX, and potentially CBR, play a role in considerably reducing ROS accumulation and oxidative damage in HL-grown cells. In agreement with this hypothesis, we have recently reported that HL-grown cells accumulate fewer PSI protein degradation products compared to LL-grown cells, suggesting they are better protected from oxidative stress (Levin et al., 2024).

High light acclimation results in PSII antenna loss

To understand the extent of PSII antenna loss, thylakoid membranes isolated from *C. ohadii* grown under LL and HL conditions were solubilized and separated by centrifugation on sucrose density gradients. As shown in Figure 2A, LL-grown cells possessed PSII-LHCII supercomplexes, as well as detached LHCII, which were visible due to the solubilization process. In contrast, the PSII-LHCII supercomplexes were absent in HL-grown *C. ohadii*, and instead, only PSII core complexes were visible on the gradient. Taken together, while the PSII-LHCII

supercomplex containing the reaction center and the accompanying antenna dominated in LL-grown cells, HL-grown cells had a PSII core devoid of the outer and inner antenna, in line with previous reports (Levin et al., 2021; Levin et al., 2023).

To understand the effect of the PSII antenna size loss on the electron transfer rate under continuous illumination, the PSII yield (Φ_{PSII}) was calculated by dividing the difference between the maximal fluorescence of cells exposed to actinic light during a saturating light pulse (F_M') and their base fluorescence (F'), by F_M' [$\Phi_{PSII} = (F_M' - F')/F_M'$], under a range of intensities (PAR). This measurement enables quantification of the relative PSII electron transfer rate (ETRII) under continuous light following the equation: ETR(II) = PAR · ETR-Factor · PPS2/PPS(1+2) · Φ_{PSII}, where PAR is the light intensity, ETR-Factor is the sample absorbance, PPS2/PPS(1+2) is the ratio of PAR absorbed by PSII to PAR absorbed by PSI and PSII and Φ_{PSII} is the PSII yield. As the absorbance differences between PSI and PSII in *C. ohadii* are unknown, a PPS2/PPS(1+2) value of 0.5, which assumes similar absorbance of the two photosystems, was used. However, the major reduction of LHCII in HL-grown cells likely significantly affects this value, resulting in distorted absolute ETRII values. Nevertheless, this calculation enabled the determination of the light intensity at which ETRII peaks in LL- and HL-grown cells. Figure 2B demonstrates that the relative ETRII was saturated in LL-cells at about 400 μmol photons m^{-2} s^{-1}, similar to other algae and plants. However, in HL-grown cells, which lack the PSII-antenna, saturation was reached at much higher light intensities, well above 1000 μmol photons m^{-2} s^{-1}, in line with previous results measured using different methods (Levin et al., 2021). This shows that the high PSII-LHCII supercomplex content in LL-grown cells versus the high PSII core complex content in HL-grown cells causes a large difference in the absorption cross-section of PSII in the two cell types.

Absence of the q_E component of NPQ in Chlorella ohadii

Since the PSII antenna in green algae and plants is a major site of reversible NPQ, this photoprotective mechanism in *C. ohadii* was investigated next. LL- and HL-grown cells were dark-adapted and then subjected to high actinic light intensity (2000 μmol photons m^{-2} s^{-1}), after which, their fluorescence parameters were recorded. Strikingly, both LL- and HL-grown cells showed a negligible NPQ response, as indicated by the limited decrease of F_M' and calculated following the equation: NPQ = (F_M/F_M')-1, where F_M and F_M' are the maximal fluorescence of dark-adapted cells or cells exposed to light, respectively, during a saturating light pulse (Figure 3A). The decreases in F_M' were minimal in *C. ohadii* compared to *C. reihardtii* tested under

similar light conditions (Figure 3A). At 2000 µmol photons m^{-2} s^{-1}, NPQ reached ~0.2 (Figure 3B), compared to ~2.3 habitually obtained in *Chlamydomonas*, owing to its strong and swift NPQ response to q_E, facilitated by the proton-sensing capabilities of LhcSR (Figure 3A). When exposed to even higher light intensities (3000 µmol photons m^{-2} s^{-1}), or when grown under strict photoautotrophic conditions, LL-grown cells developed a slightly stronger NPQ response (~0.7), while in HL-grown cells similar levels of NPQ were maintained (~0.2) (Supplemental Figures 1B, 1C, and 2). Most notably, under all tested conditions, no q_E quenching was detected in *C. ohadii*.

q_E is the major and most rapid component of NPQ which responds to light in seconds. Since it is activated by a pH decrease of the thylakoid lumen, this process was next studied in *C. ohadii*. Lumen acidification occurs due to the translocation of protons resulting from high photosynthetic electron flow under HL conditions. These protons bind conserved glutamates in LhcSR (algae) and PsbS (plants) and activate q_E. Additionally, lumen acidification activates the xanthophyll cycle. It has been shown that instead of exposing the alga to HL intensity, q_E can be triggered by artificial acidification of the lumen by the addition of acid (Tian et al., 2019). *C. ohadii* lacks the gene for LhcSR and PsbS is not expressed. However, CBR which largely accumulates in HL-cells, harbours a conserved glutamate that may function as the proton sensor activating the q_E (Levin and Schuster, 2023; Levin et al., 2023). To determine if this mechanism functions in *C. ohadii* despite the limited NPQ response, the fluorescence traces of LL and HL-grown cells were followed after artificial lumen acidification to pH 5.5 (Tian et al., 2019). In agreement with the results above, lumen acidification had little effect on the fluorescence signal, indicating the absence of q_E activation in both LL- and HL-grown *C. ohadii* cells cultured in mixotrophic (Figure 3C) or strictly photoautotrophic (Supplemental Figure 3) conditions. When the assay was applied to *C. reinhardtii* cells as a positive control, the typical fluorescence signal, indicating strong q_E and NPQ activity, was observed (Figure 3C).

The lack of q_E agrees with the absence of the lhcSR gene and the non-detectable PsbS accumulation in this alga. It mirrors the results obtained in the *C. reinhardtii* mutant which does not accumulate its major NPQ effector, LhcSR3 (Tian et al., 2019), and the psbS mutant of Arabidopsis (Wilson et al., 2024). Importantly, the results further highlight that despite a conserved glutamate (E131 in *C. ohadii*, E122 in *A. thaliana*) residue on the luminal side of the predicted CBR structure (Levin and Schuster, 2023; Levin et al., 2023), this protein does not act as a pH-induced q_E and NPQ generator. Rather, it is speculated that either it acts as a static quencher of the remaining, uncoupled LHCII in the membrane, or as a ROS-scavenging protein. Since the

xanthophyll cycle is activated and protective carotenoids are massively accumulated in HL-grown cells (Levin et al., 2021; Levin et al., 2023), it remains to be determined how these processes are activated in the absence of LhcSR and PsbS and whether or not CBR is involved.

Together, these results indicate that *C. ohadii* does not rely on NPQ mechanisms to survive when grown under intense HL. While LL-grown cells still showed some small, slowly developing NPQ effect, HL-grown cells lacked even that and both types of adapted cells lacked the q_E component of NPQ.

HL-grown cells accumulate less damaging ROS than LL-grown cells

To quantify the photoprotective capacity of the unique mechanisms in *C. ohadii*, particularly the effect of the extensive accumulation of CBR, carotenoids, and other antioxidants as well as the decrease in the PSII cross-section on a single cell level, we have employed confocal microscopy coupled with the detection of Singlet Oxygen Sensor Green (SOSG). This dye emits green fluorescence upon interaction with singlet oxygen ($^1O_2$) (Supplemented Figure 4). LL- and HL-grown cells were incubated with SOSG and exposed to 10 min of high red actinic light, followed by quantification of the accumulated $^1O_2$. HL-grown as compared to LL-grown cells accumulated significantly lower levels of $^1O_2$ (Figures 4A-C). To evaluate the contribution of $^1O_2$ that was generated via photosynthesis-related processes to this difference, we analyzed the SOSG fluorescence that was emitted specifically from within the chloroplast (Supplemented Figure 4). Analyzing 24 and 54 individual chloroplasts from LL and HL-grown cells, respectively, shows that compartmentalized analysis found that individual chloroplasts of LL-grown cells accumulated much higher levels of $^1O_2$ (Figure 4C), rising by an average of 324% increase following 10 min of red-light illumination, while in HL-grown cells, the increase was limited to an average of 175% (Figure 4C). These results are in line with the increased accumulation of O_2^- in LL-grown as compared to HL-grown algae, while the two cell types accumulated similar amounts of H_2O_2 (Figure 4D) (Levin et al., 2023). Kinetic analyses further confirmed that LL-grown cells accumulated $^1O_2$ at a significantly higher rate (Figure 5). Moreover, when observing individual chloroplasts, numerous chloroplasts of LL-grown cells accumulated tenfold more $^1O_2$ than those in HL-grown cells (Figure 4B).

To determine whether antenna properties (such as the presence of quenchers) or their abundance in the cells were at the root of these differences, $^1O_2$ production was compared between detached LHCII fractions of LL- vs. HL-grown cells at the same chlorophyll concentration (Figure 2A). Importantly, detached LHCII fractions from HL-grown cells also contain large

amounts of carotenoids and CBR, which may contribute to reduced $^1O_2$ accumulation via light quenching or direct $^1O_2$ scavenging (Levin et al., 2023). The results shown in Figure 4E demonstrate that the CBR-containing detached LHCII fractions from HL-grown cells accumulated less $^1O_2$ compared to detached LHCII fractions from LL-grown cells. However, the difference was smaller than in whole-cell measurements, suggesting that both the antenna size difference and the differences in the detached antenna properties or the accumulation of CBR and carotenoids had a paramount influence on the rate of ROS synthesis upon photosynthesis. This disparity demonstrates that the majority of the photoprotective effects are achieved through the limitation of both light absorption and $^1O_2$ accumulation. These findings may also explain the large difference in the levels of oxidized peptides between the two cell types, suggestive of higher levels of protein damage in LL-grown cells (Figure 1C).

Cyclic electron flow is highly activated in HL-grown cells

Loss of the PSII antenna creates a favorable environment for CEF around PSI (Figure 6A) (Tagawa et al., 1963; Joliot and Joliot, 2005; Alric, 2015; Nawrocki et al., 2019a). Transient measurements of P700 oxidation were made to determine whether CEF exhibited different behavior in LL- vs. HL-grown *C. ohadii*. P700 cation absorption at 830 nm serves as a proxy for the activity of CEF when the PSII is inactivated by the addition of the herbicide DCMU, or when both CEF and LEF are blocked by DBMIB - a cytochrome b_6f inhibitor (Nawrocki et al., 2019b). Drastically different behaviors of P700 oxidation were observed between the LL- and HL-grown algae (Figure 6B). When exposed to the highest tested actinic light intensities in the presence of DCMU, a long lag in P700 oxidation was noted when the cells were grown in HL, indicating high activity of CEF (Figure 6B upper panels). This lag was observed with the presence of methyl viologen, an electron acceptor from PSI, preventing back reactions. The half-time of PSI oxidation by CEF under these conditions of extremely strong illumination, as determined by the signal obtained following the addition of DCMU, reached 4 seconds, at least 4 times longer than in LL-grown *C. ohadii*, and more than one order of magnitude longer than in *Chlamydomonas* (Nawrocki et al., 2019b). Indeed, the steady state of P700 oxidation under continuous illumination – itself a commonly-used proxy for CEF activity (Takahashi et al., 2013; Alric, 2014) - at 2000 µmol photons m^{-2} s^{-1} was only around 80%, indicating that even in the absence of PSII activity, a very high rate of CEF can be maintained in *C. ohadii* adapted to HL conditions (Figure 6B). As expected, this effect was abolished when DBMIB rather than DCMU was added, demonstrating the necessity of functioning cytochrome b6f to maintain

CEF. Finally, at lower actinic light intensities in the absence of inhibitors, there was no accumulation of $P700^+$ due to its efficient reduction by PSII (Figure 6B). The effect of DCMU was visible in cells grown in LL, while no effect was detected in HL-grown *C. ohadii*, further indicating that despite illumination, a highly efficient CEF can maintain P700 mostly reduced. The inability to completely oxidize P700 at low light in the presence of DBMIB hints to additional pathways of P700+ reduction as evidenced by the relatively rapid reduction of the cation following cessation of illumination.

These functional results were strengthened by the mass spectrometry data. According to the proteomics analysis, proton gradient regulation 5 (PGR5) and PRG5-like photosynthetic phenotype 1 (PGRL1), which participate in CEF (Nawrocki et al., 2019a), accumulated in HL-grown cells (1.5-fold for both enzymes) (Figure 6C). The enhanced accumulation of ferredoxin (Fd) (3.7-fold), together with the decrease in Fd-NADP-reductase (FNR) levels (0.4-fold change), suggest a shift towards CEF rather than to LEF (Figure 6C). Given that *C. ohadii* is virtually unable to generate q_E (Figures 3A and 3B), it can be concluded that the highly active CEF in HL-grown cells did not contribute to photoprotection via the classical NPQ mechanism which is triggered by the acidification of the lumen by high activity of LEF and/or CEF. Yet, acidification of the lumen by high CEF activity can slow PQH_2 oxidation at the Qo side, resulting in the accumulation of $P700^+$, protecting PSI from over-reduction. Together, these results imply that CEF is induced and is the main electron pathway during low light exposure in HL-grown cells, while in LL-grown cells, the situation is opposite and similar to *Chlamydomonas*. CEF is also very active in HL-grown cells exposed to high light intensity. Therefore, aside from the natural requirement to balance the photosynthetic electron flow according to the imbalanced absorption cross-sections of PSII and PSI, the highly active CEF in HL-grown cells probably contributes to the most efficient photoinhibition protection mechanism.

Discussion

Extremophile species are fascinating objects of study, as their growth environments are exacerbated versions of stressful situations, rendering them models for the discovery of solutions for engineering more resistant crops. Photoprotection is thought to be a primary photosynthesis defense mechanism. NPQ is widely studied, from its molecular mechanism, through the effectors, and its influence on gene expression (for recent reviews, see (Niyogi and Truong, 2013; Murchie and Ruban, 2020; Bassi and Dall'Osto, 2021)). While NPQ pathways are widespread in most plants and algae, the current work showed that an extremely light-tolerant microalga,

C. ohadii, does not require NPQ mechanisms to thrive under extreme HL intensities (Figure 7). While growing at LL intensities, the PSII harvests light by an inner and outer antenna and generates low amounts of ROS, while containing limited levels of carotenoids (Figure 7A). When these LL-grown cells are exposed to HL intensities before being adapted to HL conditions, much more harmful ROS are produced, oxidizing and facilitating protein turnover (Figure 7B). However, in HL-grown cells that are adapted to HL conditions, the inner and outer PSII antennae are greatly reduced and several antioxidant enzymes, CBR, and a large number of carotenoids accumulate. Consequently, CEF activity is increased, resulting in much lower generation and accumulation of ROS, and therefore less protein oxidation and turnover (Figure 7C). These findings can be interpreted in the following way: Although the elimination of the LHCII in HL-grown *C. ohadii* leads to a major loss of NPQ sites, it significantly reduces the absorption cross-section of PSII. This, in turn, minimizes ROS production and together with the ROS detoxification carried out by accumulated antioxidants, reduces the rate of damage relative to the useful energy conversion (Figure 7). Alternatively, the photosynthetic proteins in HL-grown cells may indeed be damaged even under the reduced ROS conditions, yet, due to the loss of the LHCII which engulfs the PSII core proteins, they can be easily accessed to be swiftly degraded and replaced. Subsequently, there are lower levels of oxidized peptides.

Elimination of the LHCII seems like a risky strategy for photoprotection for two reasons. The first is the loss of light-harvesting capabilities during LL periods, and the second is the loss of important NPQ sites. Nonetheless, *C. ohadii* thrives in the soil crusts of the desert under direct sunlight, where few clouds or vegetation can provide shading. It is hypothesized that under these conditions of long periods of constant HL, the PSII independently absorbs sufficient light and LHCII becomes a liability due to excess energy uptake and consequent ROS production (Figure 7). Alongside LHCII elimination, the loss of NPQ in *C. ohadii* is highlighted by the absence of the LhcSR gene and PsbS protein (Treves et al., 2016; Levin et al., 2023). NPQ protects the photosystems from excess energy by swiftly modulating the energy flux between photosynthesis and regulated dissipation pathways in response to changing light. However, the present findings demonstrated that under prolonged constant HL periods in the desert, the role of NPQ seems to be dispensable.

In addition to the minimization of ROS production, the decrease in LHCII content in *C. ohadii* is accompanied by the accumulation of antioxidants such as carotenoids (Levin et al., 2021; Levin et al., 2023) and specialized enzymes, specifically GPX, SOD, and likely CBR (Figure 1A). The role of the latter protein remains elusive, but its marked accumulation (x540) in HL-grown cells suggests a central role in *C. ohadii* photoprotection (Figure 1A). Despite its

structural similarities with PsbS and LhcSR, CBR does not induce q_E or NPQ via lumen acidity sensing (Figure 3B and Supplemented Figure 3). It was suggested that CBR binds carotenoids (Levy et al., 1993) and, indeed, it was found to co-localize with carotenoids and the detached LHCII fraction of HL-grown *C. ohadii* (Levin et al., 2023). Carotenoids are efficient ROS scavengers (Triantaphylidès and Havaux, 2009), and CBR may contribute to these activities while it is bound to carotenoids. Moreover, the significant accumulation of carotenoids in the thylakoid membrane of HL-grown *C. ohadii*, predominantly zeaxanthin, and lutein, may contribute to this effect (Levin et al., 2023). In addition to being a ROS target, CBR may be an internal UV light screen, expressed by the cells to prevent donor-side damage to PSII.

The overall level of detectable ROS was significantly decreased upon illumination of HL-grown alga. Given the elimination of the PSII antenna and antioxidant accumulation, it is likely that the decline in ROS levels is a product of the smaller absorption cross-section and of the detoxifying effect of the upregulated ROS-scavenging enzymes (Figure 7). More specifically, the smaller cross-section results in a mild decrease in the amount of absorbed light, which limits ROS synthesis (Santabarbara et al., 1999; Santabarbara et al., 2001). Then, the decreased concentration of nascent ROS due to scavenging activity or using CBR-bound carotenoids as an oxidation target, minimizes the overall accumulation of these deleterious species.

Finally, CEF around PSI is often thought of as a transitory process that occurs before the Calvin-Benson cycle becomes active at the onset of illumination. The finding that CEF is highly active in HL-grown *C. ohadii* suggests that it may play another role in this alga. It is speculated that CEF in *C. ohadii* enhances ATP synthesis, needed due to the high rates of photoinhibition under desert growth conditions and the heavy energetic cost of PSII repair. Surprisingly, little or no lumen acidification-induced NPQ was detected in the alga (Figure 3B), suggesting that the highly active CEF is not used to boost PSII photoprotection by the classic NPQ mechanism. Additionally, P700 is primarily maintained in its neutral form even under high light (Figure 6B). These findings suggest that CEF is also employed by HL-grown *C. ohadii* to protect PSI from over-reduction. Yet, the mechanism of this photoprotective role remains unknown.

It is a long-standing technical difficulty in the field of functional photosynthesis to ascertain that transient CEF in the absence of PSII activity – as is the case in our measurements – reflects the situation when LEF is functioning (Fan et al., 2016). The long-lived CEF at the onset of illumination in *C. ohadii* could nonetheless serve as a model for the development of novel methodologies for its quantification, a critical feat for photosynthesis physiology in the coming years.

To conclude, NPQ is not essential for photoprotection in the extremophilic green algae, *C. ohadii*, and it is redundant under constant exposure to extreme HL. This work expanded the understanding of photoprotection at the frontier of survivability and provided promising targets for enhancing photoinhibition resistance and yields of important crops via genetic tools (Figure 7).

Materials and Methods

Cell culture and acclimation to low or high light conditions

Log-phase *Chlorella ohadii* cells were diluted to optical density $(OD)_{750nm}$ 0.2 in a final volume of 400 ml tris-acetate phosphate (TAP) medium and then split: 200 ml were placed under LL (50 µmol photons m^{-2} s^{-1}) conditions and 200 ml were placed under HL (2,000 µmol photons m^{-2} s^{-1}) conditions, in 1 L Erlenmeyer under shaking (100 rpm), for 24 h, at 28 °C. To prevent self-shading, the cells were maintained below an OD_{750nm} value of 0.8 by diluting them to OD_{750nm} 0.2 every 8 h during the growth period. After 24 h, the LL- and HL-grown cells were harvested for further experimentation. For experiments under strict photoautotrophic conditions, the cells were grown in a tris-phosphate (TP) medium, with no acetate as a carbon source.

Photosynthetic complex separation by sucrose density gradient centrifugation

LL- and HL-grown cells were pelleted and washed twice with sucrose (300 mM)-tris-tricine (15 mM each pH 8)-$NaCl_2$ (15 mM) (STN) buffer. The cells were broken in a MicroFluidizer (50 psi); unbroken cells were pelleted (15,000 g, 10 min, 4 °C). The supernatant was collected and thylakoid membranes were pelleted in an ultracentrifuge (250,000g, 2 h, 4 °C). Thylakoid membranes were resuspended in 25 mM MES (pH 6.5) to a chlorophyll concentration of 0.2 or 0.4 mg/ml for LL- or HL-grown samples, respectively, and solubilized with 1% n-dodecyl-α-D-maltopyranoside (α-DDM) for 15 min, on ice, under dark conditions. Insolubilized material was pelleted (9,500 g, 10 min, 4 °C) and the supernatant was loaded on a sucrose density gradient (20 mM MES pH 6.5, 0.02% α-DDM, 4%-45% sucrose). Individual complexes were separated by ultracentrifugation (100,000 g, 20 h, 4 °C)

Sample preparation for photosynthetic parameter analysis

LL- and HL-grown cells were pelleted and resuspended in fresh medium to the equivalent of 10 µg/ml chlorophyll for PSII chlorophyll fluorescence analysis, or 50 µg/ml for P700 (PSI) absorption analysis. The cells were dark-adapted for at least 30 min with air bubbling, then

loaded to a quartz cuvette and analyzed with a Dual-PAM-100 fluorometer (Walz, Germany). Red actinic light was used in all measurements.

Creation of a PSII electron transport rate saturation curve

After exposure of LL- and HL-grown cells to different light intensities for 30 sec, the PSII operating efficiency (Φ_{PSII}) was measured using the following the equation: $\Phi_{PSII} = (F_M'-F')/F_M'$. PSII ETR was calculated following the equation: ETR(II) = PAR · ETR-Factor · PPS2/PPS(1+2) · ΦPSII, where PAR is the light intensity, the ETR-Factor is the sample absorbance, the PPS2/PPS(1+2) is the ratio of PAR absorbed by PSII to PAR absorbed by PSI and PSII (assumed to be 0.5 in the present analysis) and Φ_{PSII} is the PSII yield.

NPQ analysis

The fluorescence traces of LL- and HL-grown cells were monitored upon exposure to various light intensities (50, 400, 2000, and 3000 µmol photons m^{-2} s^{-1}) for 10 min, followed by 3 min of darkness for recovery. When indicated, acetic acid (1 mM final) was added directly to the cuvette to induce q_E (Tian et al., 2019). NPQ was calculated following the equation: NPQ = $(F_M/F_M')-1$

P700 activity and cyclic electron flow

P700 oxidation kinetics was monitored in LL- and HL-grown cells upon illumination with various light intensities: 50, 400, or 2000 µmol photons m^{-2} s^{-1}, in the presence or absence of the photosynthetic electron transfer inhibitors 3-(3,4-dichlorophenyl)-1,1-dimethylurea (100 µM, DCMU) or 2,5-dibromo-3-methyl-6-isopropylbenzoquinone (100 µM, DBMIB). Methyl viologen (6 mM) was added to all samples to prevent charge recombination in PSI.

ROS accumulation measurements

Live-cell $^1O_2$ quantification with singlet oxygen sensor green

LL- and HL-grown *C. ohadii* cells were pelleted and resuspended to OD_{750nm} 0.2 in TAP medium containing 50µM singlet oxygen sensor green (SOSG). Subsequently, the cells were incubated for 30 min under LL conditions, at 28°C, and pelleted and resuspended in fresh TAP medium. To visualize the formation of $^1O_2$, the cells were loaded to a spinning disk confocal microscope (Nikon Eclipse Ti2, Confocal scanner unit Yokogawa CSU-W1, Camera Photometrics PrimΣ-BSI). HL stimulation was achieved using a red LED integrated into the microscope, providing an intensity of 3.9 mW (660 nm) for a duration of 1-10 min. The SOSG was

excited at 488 nm, and the fluorescence emission was recorded at 530 nm. Chlorophyll fluorescence was recorded with excitation at 430 nm and emission at 680 nm to identify the chloroplasts. IMARIS software (Oxford Instruments) was employed to reconstruct the chloroplast structure based on the chlorophyll fluorescence. Subsequently, only SOSG fluorescence that corresponded to the reconstructed chloroplast was measured, ensuring a specific and accurate assessment of the effects of light stress on the observed photosynthetically derived $^1O_2$ formation. The graphs were prepared with the R environment for statistical computing and graphics (https://www.R-project.org/) using the ggplot2 package (Wickham, 2016). The linear mixed model was calculated with the lme4 package (Bates et al., 2015). SEs and post-hoc analysis were calculated using the emmeans package (https://CRAN.R-project.org/package=emmeans). Mixed-model ANOVA was used to determine statistical significance (see Figure 5B)

$^1O_2$ accumulation in isolated LHCII complexes

Isolated LHCII from LL-grown cells and isolated LHCII together with CBR from HL-grown cells were resuspended in STNM buffer (50 mM Tricine-KOH pH 7.6, 15mM $NaCl_2$, 300 mM sucrose, and 5mM $MgCl_2$) with SOSG (10 µM) to a final chlorophyll concentration of 0.028 µg/µl. The samples were loaded onto a black 96-well plate and SOSG fluorescence was measured before and after 10 min of HL illumination in a fluorescence plate reader (ClarioStar 500, BMG Labtech, Ortenberg, Germany) with excitation at 488 nm and an emission range of 530-600nm. The samples were placed on ice during the illumination period to avoid protein denaturation. STNM buffer with SOSG was used as a blank to measure and exclude the background SOSG fluorescence. Three biological repeats were tested for each treatment condition.

O^{2-} and H_2O_2 accumulation in low-light- and high-light-grown C. ohadii cells

Nitro-blue tetrazolium (NBT), which upon reduction creates blueish–greyish insoluble precipitates, and 3,3′-diaminobenzidine (DAB), which upon oxidation by H_2O_2 is colored dark brown, were used to measure O^{2-} and H_2O_2 accumulation in LL- and HL-grown *C. ohadii* cells. The cell OD_{750nm} was adjusted to 0.7. One milliliter of each sample was subjected to a 10-min incubation under HL conditions, with the addition of either 5 mM NBT or 5 mM DAB. Thereafter, chlorophyll was extracted with 100% methanol, at 40 °C. Cells were then pelleted (3000 g, 5 min), and resuspended in 200 µl methanol (100%). The resulting cell suspension was applied as spots onto the Whatman 3 paper filter. ROS were quantified in ImageJ, based on the color intensity.

Mass spectrometry whole-cell sample preparation and proteolysis

Three biological repeats of LL- and HL-grown *C. ohadii* cells were harvested, washed twice with STN, and broken under 50 psi with a MicroFluidizer. Samples were suspended in 8.5 M urea, 100 mM ammonium bicarbonate, and 10 mM DTT. Protein content was estimated using Bradford readings. The samples were reduced (60 ºC, 30 min), modified with 35.2 mM iodoacetamide in 100 mM ammonium bicarbonate (room temperature for 30 min in the dark), and digested in 1.5 M urea and 17.6 mM ammonium bicarbonate with modified trypsin (Promega), overnight, at 37 °C, at a 1:50 (M/M) enzyme-to-substrate ratio. A second digestion with trypsin was performed for 4 h, at 37 °C, at a 1:100 (M/M) enzyme-to-substrate ratio. The tryptic peptides were desalted using Oasis HLB 96-well µElution Plate (Waters), dried, and re-suspended in 0.1% formic acid.

Mass spectrometry analysis

The resulting peptides were analyzed by LC-MS/MS using a Q Exactive HFX mass spectrometer (Thermo) fitted with an HPLC capillary (Ultimate 3000, Thermo Scientific). The peptides were loaded in solvent A (0.1% formic acid in water) on a homemade capillary column (30 cm, 75-micron ID) packed with Reprosil C18-Aqua (Dr. Maisch GmbH, Germany). The peptide mixture was resolved with a 5-28% linear gradient of solvent B (99.99% acetonitrile with 0.1% formic acid) for 180 min, followed by a gradient of 28-95% for 15 min, and then 15 minutes at 95% acetonitrile with 0.1% formic acid in water at flow rates of 0.15 µl/min. Mass spectrometry was performed in a positive mode (m/z 350-1200, resolution 120,000 for MS1 and 15,000 for MS2), using repetitively full MS scan followed by high collision dissociation (HCD, at 27 normalized collision energy) of the 30 most-dominant ions (>1 charges) selected from the first MS scan. The AGC settings were $3x10^6$ for the full MS and $1x10^5$ for the MS/MS scans. A dynamic exclusion list was enabled with an exclusion duration of 20 s.

Mass spectrometry data analysis

Raw data was processed with MaxQuant version 2.5.2 (Tyanova et al., 2016) for protein accumulation analysis and MSfragger version 4.0 (Kong et al., 2017) via FragPipe version 21.1 (https://fragpipe.nesvilab.org/) for detection of tryptophan oxidized peptides. In the absence of a fully annotated proteome for *C. ohadii*, we utilized a combined dataset of protein sequences in our identification process. This dataset includes all available Chlorella protein sequences

(Tax ID = 3701) downloaded from UniProt as of July 2019, comprising a total of 20973 sequences. Additionally, we incorporated all available *C. ohadii* protein sequences (11470) from NCBI, as downloaded on October 2023. All searches included enzymatic cleavage with trypsin (cleavage after K/R but not P) and two missed cleavages and a clip of N-term methionine unless specified otherwise. Cysteine carbamidomethyl (+57.02146) was set as a fixed modification, and methionine oxidation (+15.994915) and protein N-terminal acetylation were set as variable modifications.

MaxQuant searches were performed using tryptic digestion mode with a minimal peptide length of 7 amino acids. Search criteria included up to 2 missed cleavages, precursor and fragments tolerance of 20 ppm, oxidation of methionine, and protein N-terminal acetylation set as variable modifications. Default settings were used for all other parameters. Candidates were filtered to obtain an FDR of 1% at the peptide and protein levels. For quantification, the match between runs (MBR) module of MaxQuant was used with the Label-Free Quantification (LFQ) normalization method enabled.

Identification and quantification of tryptophan oxidation was performed using FragPipe's 'LFQ-MBR' workflow. The workflow default settings were used with the additions of tryptophan oxidation (+15.994915) and deoxidation (+31.989829) as variable modifications for identifying tryptophan oxidation.

Further analysis was performed using the Perseus software v.2.0.11 (Tyanova et al., 2016). Label-free quantification (LFQ) intensity values were used to calculate the relative abundance of total proteins and tryptophan oxidized peptides in LL and HL whole-cell samples. The results were filtered to exclude contaminants, reverse, and only identified by site proteins. Label-free quantification values were transformed (Log2) and filtered to include only proteins that were detected in three repeats of at least one group: LL or HL samples. Missing values were then added from a normal distribution (https://cox-labs.github.io/coxdocs/replacemissingfromgaussian.html). A two-sample t-test was used to determine the statistical significance of differences between groups, applying a permutation-based false discovery rate (FDR) of 0.05 and an S0 parameter of 0.1. Intensity-based absolute quantification (iBAQ) (Schwanhäusser et al., 2011) was used to determine the abundance of a given protein in HL-grown cells. A protein with a higher iBAQ value is more abundant compared to a protein with a low iBAQ value. The proteins were listed according to their average iBAQ values (high to low) in HL-grown cells. The percentile of the protein was determined by dividing its number (position) on the list, by

the total number of proteins, and multiplying by 100. For example, if protein X is 40th on the list, and a total of 4000 proteins were detected in the analysis, then protein X is in the 1st percentile, i.e. in the top 1% most abundant proteins in the cell.

Data availability

The mass spectrometry proteomics RAW data have been deposited to the ProteomeXchange Consortium via the PRIDE (Perez-Riverol et al., 2022) partner repository with the dataset identifier will be provided once available.

Funding:

Funding was provided by an Israel Science Foundation (ISF) grant (2199/22).

Author contributions: GL, GS, FAW, and WN planned the research and wrote this manuscript. GL and MS performed the experiments and data analysis unless stated otherwise. OK and RH assisted with proteomics data analysis. GH helped analyze the singlet oxygen accumulation data and performed statistical analyses. OL assisted with NPQ measurements.

Acknowledgments:

We thank Dr. Nitzan Dahan from the Technion LS&E microscopy unit for his assistance and guidance. We thank the Smoler Proteomics Center at the Technion for performing the mass spectrometry experiments. We thank Nir Keren and Iftach Yacobi for their helpful advice and discussions.

Declaration of interests:

The authors declare no competing interests.

Dedication

This paper is dedicated to the late Professor Itzhak Ohad, an outstanding and beloved scientist and mentor, who made a substantial contribution to our understanding of photoinhibition and paved the way to the isolation of *C. ohadii*.

References

Allorent, G., Tokutsu, R., Roach, T., Peers, G., Cardol, P., Girard-Bascou, J., Seigneurin-Berny, D., Petroutsos, D., Kuntz, M., Breyton, C., et al. (2013). A Dual Strategy to Cope with High Light in *Chlamydomonas reinhardtii*. *The Plant Cell* 25:545–557.

Alric, J. (2014). Redox and ATP control of photosynthetic cyclic electron flow in Chlamydomonas reinhardtii. *Biochimica et Biophysica Acta (BBA) - Bioenergetics* 1837:825–834.

Alric, J. (2015). The plastoquinone pool, poised for cyclic electron flow? *Front. Plant Sci.* 6.

Bag, P., Shutova, T., Shevela, D., Lihavainen, J., Nanda, S., Ivanov, A. G., Messinger, J., and Jansson, S. (2023). Flavodiiron-mediated O2 photoreduction at the photosystem I acceptor-side provides photoprotection to conifer thylakoids in early spring. *Nat Commun* 14:3210.

Bassi, R., and Dall'Osto, L. (2021). Dissipation of Light Energy Absorbed in Excess: The Molecular Mechanisms. *Annu. Rev. Plant Biol.* 72:47–76.

Bates, D., Mächler, M., Bolker, B., and Walker, S. (2015). Fitting Linear Mixed-Effects Models Using lme4. *J. Stat. Soft.* 67.

Bonaventura, C., and Myers, J. (1969). Fluorescence and oxygen evolution from Chlorella pyrenoidosa. *Biochimica et Biophysica Acta (BBA) - Bioenergetics* 189:366–383.

Burlacot, A., Dao, O., Auroy, P., Cuiné, S., Li-Beisson, Y., and Peltier, G. (2022). Alternative photosynthesis pathways drive the algal CO2-concentrating mechanism. *Nature* 605:366–371.

Calzadilla, P. I., Song, J., Gallois, P., and Johnson, G. N. (2024). Proximity to Photosystem II is necessary for activation of Plastid Terminal Oxidase (PTOX) for photoprotection. *Nat Commun* 15:287.

Chow, W., Telfer, A., Chapman, D. J., and Barber, J. (1981). State 1-state 2 transition in leaves and its association with ATP-induced chlorophyll fluorescence quenching. *Biochimica et Biophysica Acta (BBA) - Bioenergetics* 638:60–68.

Delosme, R. (1967). Étude de l'induction de fluorescence des algues vertes et des chloroplastes au début d'une illumination intense. *Biochimica et Biophysica Acta (BBA) - Bioenergetics* 143:108–128.

Delosme, R., Olive, J., and Wollman, F.-A. (1996). Changes in light energy distribution upon state transitions: an in vivo photoacoustic study of the wild type and photosynthesis mutants from Chlamydomonas reinhardtii. *Biochimica et Biophysica Acta (BBA) - Bioenergetics* 1273:150–158.

Demmig, B., Winter, K., Krüger, A., and Czygan, F.-C. (1987). Photoinhibition and Zeaxanthin Formation in Intact Leaves: A Possible Role of the Xanthophyll Cycle in the Dissipation of Excess Light Energy. *Plant Physiol.* 84:218–224.

Demmig-Adams, B., Winter, K., Krüger, A., and Czygan, F.-C. (1989). Zeaxanthin Synthesis, Energy Dissipation, and Photoprotection of Photosystem II at Chilling Temperatures. *Plant Physiol.* 90:894–898.

Demmig-Adams, B., Adams, W. W., Heber, U., Neimanis, S., Winter, K., Krüger, A., Czygan, F.-C., Bilger, W., and Björkman, O. (1990). Inhibition of Zeaxanthin Formation and of Rapid Changes in Radiationless Energy Dissipation by Dithiothreitol in Spinach Leaves and Chloroplasts. *Plant Physiol.* 92:293–301.

Elrad, D., Niyogi, K. K., and Grossman, A. R. (2002). A Major Light-Harvesting Polypeptide of Photosystem II Functions in Thermal Dissipation[W]. *The Plant Cell* 14:1801–1816.

Fan, D.-Y., Fitzpatrick, D., Oguchi, R., Ma, W., Kou, J., and Chow, W. S. (2016). Obstacles in the quantification of the cyclic electron flux around Photosystem I in leaves of C3 plants. *Photosynth Res* 129:239–251.

Joliot, P., and Joliot, A. (2005). Quantification of cyclic and linear flows in plants. *Proc. Natl. Acad. Sci. U.S.A.* 102:4913–4918.

Kato, Y., Kuroda, H., Ozawa, S.-I., Saito, K., Dogra, V., Scholz, M., Zhang, G., de Vitry, C., Ishikita, H., Kim, C., et al. (2023). Characterization of Tryptophan Oxidation Affecting D1 Degradation by FtsH in the Photosystem II Quality Control of Chloroplasts. *elife* https://doi.org/10.7554/eLife.88822.3.

Kong, A. T., Leprevost, F. V., Avtonomov, D. M., Mellacheruvu, D., and Nesvizhskii, A. I. (2017). MSFragger: ultrafast and comprehensive peptide identification in mass spectrometry–based proteomics. *Nat Methods* 14:513–520.

Levin, G., and Schuster, G. (2023). LHC-like Proteins: The Guardians of Photosynthesis. *IJMS* 24:2503.

Levin, G., Kulikovsky, S., Liveanu, V., Eichenbaum, B., Meir, A., Isaacson, T., Tadmor, Y., Adir, N., and Schuster, G. (2021). The desert green algae *Chlorella ohadii* thrives at excessively high light intensities by exceptionally enhancing the mechanisms that protect photosynthesis from photoinhibition. *The Plant Journal* 106:1260–1277.

Levin, G., Yasmin, M., Liveanu, V., Burstein, C., Hanna, R., Kleifeld, O., Simanowitz, M. C., Meir, A., Tadmor, Y., Hirschberg, J., et al. (2023). A desert *Chlorella* sp. that thrives at extreme high-light intensities using a unique photoinhibition protection mechanism. *The Plant Journal* 115:510–528.

Levin, G., Yasmin, M., Pieńko, T., Yehishalom, N., Hanna, R., Kleifeld, O., Glaser, F., and Schuster, G. (2024). The protein phosphorylation landscape in photosystem I of the desert algae *Chlorella* sp. *New Phytologist* Advance Access published February 21, 2024, doi:10.1111/nph.19603.

Levy, H., Tal, T., Shaish, A., and Zamir, A. (1993). Cbr, an algal homolog of plant early light-induced proteins, is a putative zeaxanthin binding protein. *Journal of Biological Chemistry* 268:20892–20896.

Li, X.-P., Björkman, O., Shih, C., Grossman, A. R., Rosenquist, M., Jansson, S., and Niyogi, K. K. (2000). A pigment-binding protein essential for regulation of photosynthetic light harvesting. *Nature* 403:391–395.

Li, X.-P., Gilmore, A. M., Caffarri, S., Bassi, R., Golan, T., Kramer, D., and Niyogi, K. K. (2004). Regulation of Photosynthetic Light Harvesting Involves Intrathylakoid Lumen pH Sensing by the PsbS Protein. *Journal of Biological Chemistry* 279:22866–22874.

Liguori, N., Roy, L. M., Opacic, M., Durand, G., and Croce, R. (2013). Regulation of Light Harvesting in the Green Alga *Chlamydomonas reinhardtii* : The C-Terminus of LHCSR Is the Knob of a Dimmer Switch. *J. Am. Chem. Soc.* 135:18339–18342.

Murchie, E. H., and Ruban, A. V. (2020). Dynamic non-photochemical quenching in plants: from molecular mechanism to productivity. *The Plant Journal* 101:885–896.

646 Murik, O., Geffen, O., Shotland, Y., Fernandez-Pozo, N., Ullrich, K. K., Walther, D., Rensing, S. A., and
647 Treves, H. (2024). Genomic imprints of unparalleled growth. *New Phytologist* 241:1144–
648 1160.

649 Nawrocki, W. J., Santabarbara, S., Mosebach, L., Wollman, F.-A., and Rappaport, F. (2016). State
650 transitions redistribute rather than dissipate energy between the two photosystems in Chla-
651 mydomonas. *Nat. Plants* 2:16031.

652 Nawrocki, W. J., Bailleul, B., Picot, D., Cardol, P., Rappaport, F., Wollman, F.-A., and Joliot, P. (2019a).
653 The mechanism of cyclic electron flow. *Biochimica et Biophysica Acta (BBA) - Bioenergetics*
654 1860:433–438.

655 Nawrocki, W. J., Bailleul, B., Cardol, P., Rappaport, F., Wollman, F.-A., and Joliot, P. (2019b). Maximal
656 cyclic electron flow rate is independent of PGRL1 in Chlamydomonas. *Biochimica et Biophys-*
657 *ica Acta (BBA) - Bioenergetics* 1860:425–432.

658 Nicol, L., and Croce, R. (2021). The PsbS protein and low pH are necessary and sufficient to induce
659 quenching in the light-harvesting complex of plants LHCII. *Sci Rep* 11:7415.

660 Niyogi, K. K., and Truong, T. B. (2013). Evolution of flexible non-photochemical quenching mecha-
661 nisms that regulate light harvesting in oxygenic photosynthesis. *Current Opinion in Plant Bi-*
662 *ology* 16:307–314.

663 Niyogi, K. K., Grossman, A. R., and Björkman, O. (1998). Arabidopsis Mutants Define a Central Role
664 for the Xanthophyll Cycle in the Regulation of Photosynthetic Energy Conversion. *The Plant*
665 *Cell* 10:1121–1134.

666 Ögren, E. (1988). Photoinhibition of photosynthesis in willow leaves under field conditions. *Planta*
667 175:229–236.

668 Ögren, E., and Sjöström, M. (1990). Estimation of the effect of photoinhibition on the carbon gain in
669 leaves of a willow canopy. *Planta* 181.

670 Peers, G., Truong, T. B., Ostendorf, E., Busch, A., Elrad, D., Grossman, A. R., Hippler, M., and Niyogi,
671 K. K. (2009). An ancient light-harvesting protein is critical for the regulation of algal photo-
672 synthesis. *Nature* 462:518–521.

673 Perez-Riverol, Y., Bai, J., Bandla, C., García-Seisdedos, D., Hewapathirana, S., Kamatchinathan, S.,
674 Kundu, D. J., Prakash, A., Frericks-Zipper, A., Eisenacher, M., et al. (2022). The PRIDE data-
675 base resources in 2022: a hub for mass spectrometry-based proteomics evidences. *Nucleic*
676 *Acids Research* 50:D543–D552.

677 Ruban, A. V., Lee, P. J., Wentworth, M., Young, A. J., and Horton, P. (1999). Determination of the
678 Stoichiometry and Strength of Binding of Xanthophylls to the Photosystem II Light Harvest-
679 ing Complexes. *Journal of Biological Chemistry* 274:10458–10465.

680 Sacharz, J., Giovagnetti, V., Ungerer, P., Mastroianni, G., and Ruban, A. V. (2017). The xanthophyll
681 cycle affects reversible interactions between PsbS and light-harvesting complex II to control
682 non-photochemical quenching. *Nature Plants* 3:16225.

683 Santabarbara, S., Garlaschi, F. M., Zucchelli, G., and Jennings, R. C. (1999). The effect of excited state
684 population in Photosystem II on the photoinhibition-induced changes in chlorophyll fluores-
685 cence parameters. *Biochimica et Biophysica Acta* 1409:165–170.

686 Santabarbara, S., Neverov, K. V., Garlaschi, F. M., Zucchelli, G., and Jennings, R. C. (2001). Involve-
687 ment of uncoupled antenna chlorophylls in photoinhibition in thylakoids. *FEBS Letters*
688 491:109–113.

689 Schmid-Siegert, E., Stepushenko, O., Glauser, G., and Farmer, E. E. (2016). Membranes as Structural
690 Antioxidants. *Journal of Biological Chemistry* 291:13005–13013.

691 Schwanhäusser, B., Busse, D., Li, N., Dittmar, G., Schuchhardt, J., Wolf, J., Chen, W., and Selbach, M.
692 (2011). Global quantification of mammalian gene expression control. *Nature* 473:337–342.

693 Tagawa, K., Tsujimoto, H. Y., and Arnon, D. I. (1963). ROLE OF CHLOROPLAST FERREDOXIN IN THE EN-
694 ERGY CONVERSION PROCESS OF PHOTOSYNTHESIS. *Proc. Natl. Acad. Sci. U.S.A.* 49:567–572.

695 Takahashi, H., Clowez, S., Wollman, F.-A., Vallon, O., and Rappaport, F. (2013). Cyclic electron flow is
696 redox-controlled but independent of state transition. *Nat Commun* 4:1954.

697 Tian, L., Nawrocki, W. J., Liu, X., Polukhina, I., van Stokkum, I. H. M., and Croce, R. (2019). pH depend-
698 ence, kinetics and light-harvesting regulation of nonphotochemical quenching in *Chlamydo-*
699 *monas*. *Proc. Natl. Acad. Sci. U.S.A.* 116:8320–8325.

700 Treves, H., Raanan, H., Finkel, O. M., Berkowicz, S. M., Keren, N., Shotland, Y., and Kaplan, A. (2013).
701 A newly isolated *Chlorella* sp. from desert sand crusts exhibits a unique resistance to excess
702 light intensity. *FEMS Microbiol Ecol* 86:373–380.

703 Treves, H., Raanan, H., Kedem, I., Murik, O., Keren, N., Zer, H., Berkowicz, S. M., Giordano, M., Norici,
704 A., Shotland, Y., et al. (2016). The mechanisms whereby the green alga *Chlorella ohadii* , iso-
705 lated from desert soil crust, exhibits unparalleled photodamage resistance. *New Phytol*
706 210:1229–1243.

707 Triantaphylidès, C., and Havaux, M. (2009). Singlet oxygen in plants: production, detoxification and
708 signaling. *Trends in Plant Science* 14:219–228.

709 Tyanova, S., Temu, T., Sinitcyn, P., Carlson, A., Hein, M. Y., Geiger, T., Mann, M., and Cox, J. (2016).
710 The Perseus computational platform for comprehensive analysis of (prote)omics data. *Nat*
711 *Methods* 13:731–740.

712 Wickham, H. (2016). *ggplot2: Elegant Graphics for Data Analysis*. 2nd ed. Cham: Springer Interna-
713 tional Publishing.

714 Wilson, S., Clarke, C. D., Carbajal, M. A., Buccafusca, R., Fleck, R. A., Daskalakis, V., and Ruban, A. V.
715 (2024). Hydrophobic Mismatch in the Thylakoid Membrane Regulates Photosynthetic Light
716 Harvesting. *Journal of the American Chemical Society* Advance Access published 2024,
717 doi:https://doi.org/10.1021/jacs.4c05220.

718 Wolff, Ch., and Witt, H. T. (1969). On Metastable States of Carotenoids in Primary Events of Photo-
719 synthesis: — Registration by repetitive ultra-short-flash photometry —. *Zeitschrift für*
720 *Naturforschung B* 24:1031–1037.

721 Xu, P., Tian, L., Kloz, M., and Croce, R. (2015). Molecular insights into Zeaxanthin-dependent quench-
722 ing in higher plants. *Sci Rep* 5:13679.

723

Figures and figure legends

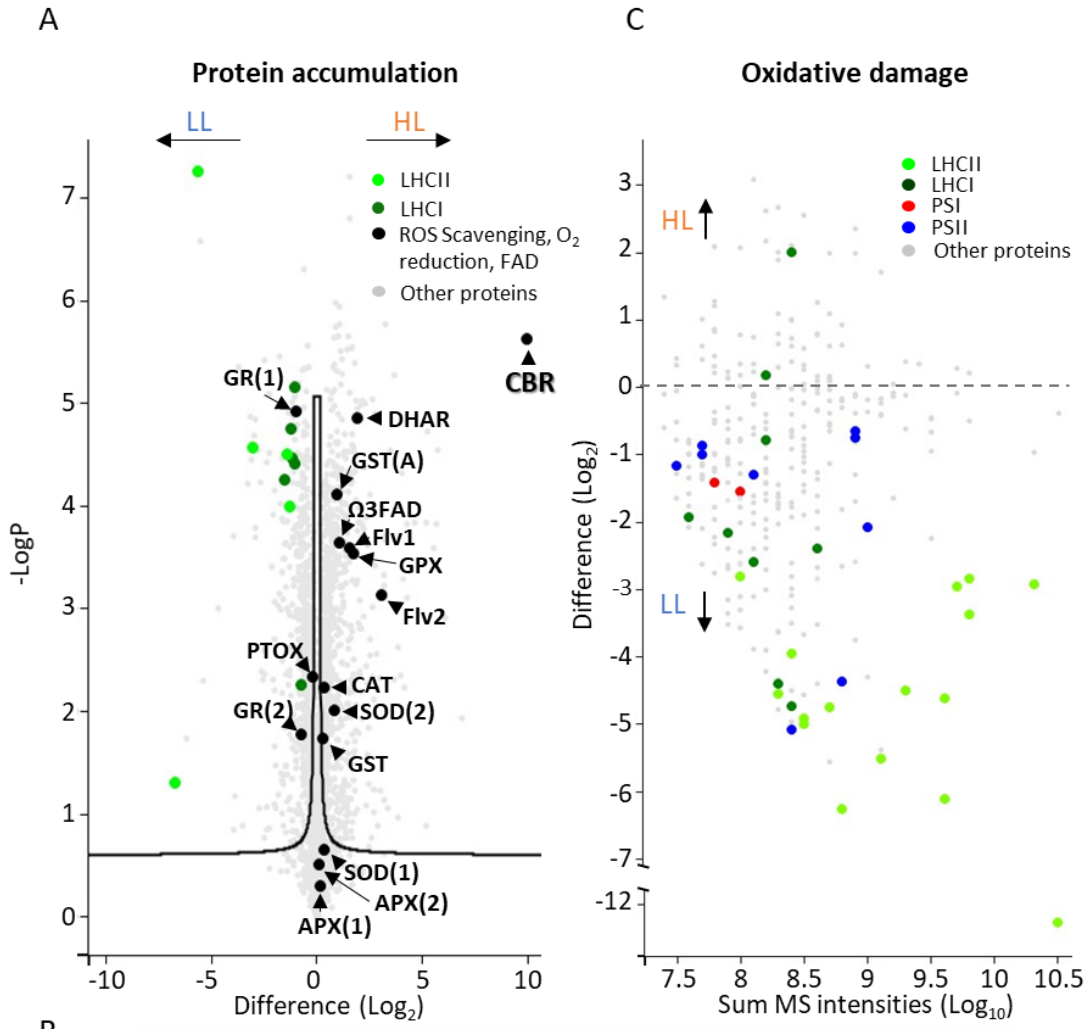

B

Protein	Function	LFQ HL/LL	Percentile in HL (iBAQ)
SOD (2)	O_2- detoxification	1.8	0.7
GPX	Glut. Cycle	3.3	6.7
CBR	?	994.5	7.9
SOD (1)	O_2- detoxification	1.3	9.1
Ω3FAD	PUFA detoxification	2.1	11.5
GR (2)	Glut. Cycle	0.6	13.8
Catalase	H_2O_2 detoxification	1.3	21.7
DHAR	Glut. Cycle	3.8	21.8
Flv1	O_2-> H_2O	2.9	25.7
GR (1)	Glut. Cycle	0.5	25.9
Flv2	O_2-> H_2O	8.4	34.2
GST	Glut. Cycle	1.2	38.9
GST(A)	Glut. Cycle	1.9	41.9
APX (1)	Glut. Cycle	1.1	42.7
APX (2)	Glut. Cycle	1.1	46.4
PTOX	O_2-> H_2O	0.9	51.6

Figure 1. Accumulation of antioxidants correlates with reduced oxidative damage in high-light-grown *Chlorella ohadii*.

(A) Label-free quantification (LFQ) Liquid chromatography-tandem mass spectrometry (LC-MS/MS) in low and high light (LL and HL)-grown cells reveals the accumulation of known enzymatic antioxidants and CBR in HL-grown cells. Note the substantial reduction in LHCII subunits in HL-grown *C. ohadii*.

(B) List of the detected antioxidants and other related enzymes. Values in the 'LFQ HL/LL' column represent the fold-change value of a given protein in HL over LL-grown cells. Values in the 'Percentile in HL (iBAQ)' column represent the abundance of the protein within HL-grown cells. A value of 10 means this protein is amongst the 10% most abundant proteins in these cells.

(C) Detected peptides with oxidized tryptophan as a mark for oxidative damage. Note the accumulation of almost all detected oxidized peptides in LL-grown cells.

SOD – Superoxide dismutase. GPX – Glutathione peroxidase. CBR – Carotenoid biosynthesis related. Ω3FAD – omega 3 fatty acid desaturase. GR – Glutathione reductase. DHAR - Dehydroascorbate reductase. FLV – Flavodiiron protein. APX – Ascorbate peroxidase. GST – Glutathione S transferase. PTOX – Plastid/Plastoquinol terminal oxidase.

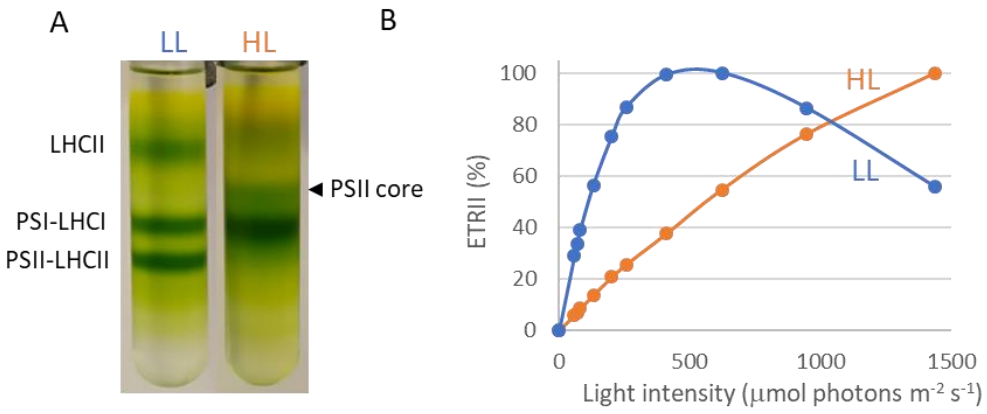

Figure 2. High light-grown *Chlorella ohadii* truncates the photosystem II antenna.

(A) Thylakoid membranes from low and high-light (LL and HL) grown cells were solubilized with detergents and the photosynthetic complexes were separated by a sucrose density gradient centrifugation. Samples containing the same amount of chlorophyll (200 µg) were loaded on the gradients. Note the accumulation of a PSII core, stripped from LHCII, in HL-grown cells.

(B) The relative electron transport rates of photosystem II (ETRII) were normalized as described in the text and tested under various light intensities. To avoid bias due to incorrect antennae sizes, values are provided as a percentage (%) of maximal ETRII rather than in absolute values. In HL-grown *C. ohadii*, ETRII does not reach peak values even at the highest light intensities used here due to its truncated photosystem II antenna.

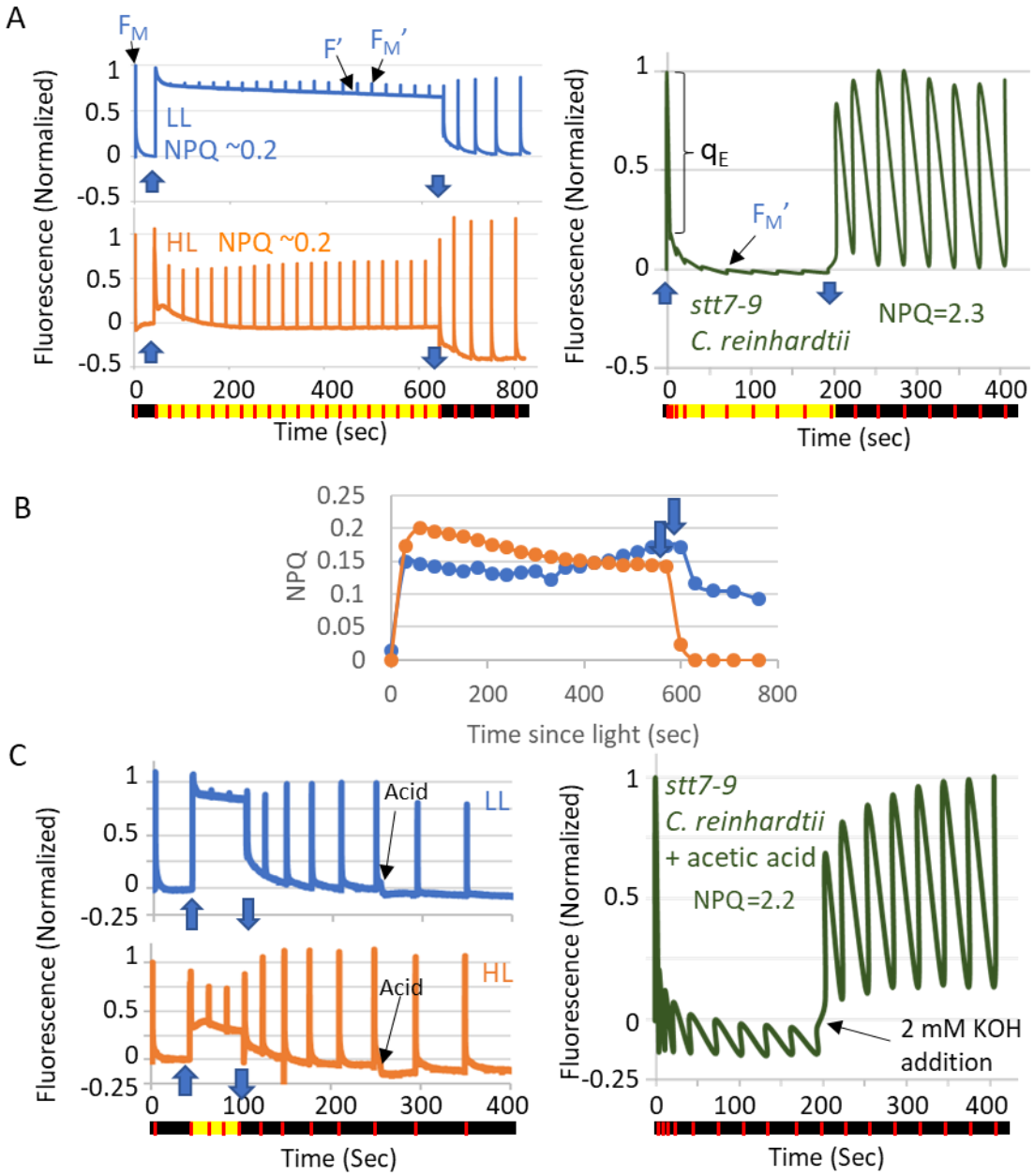
A
F_M
F'
F_M'
LL
NPQ ~0.2
HL NPQ ~0.2
Fluorescence (Normalized)
Time (sec)
q_E
F_M'
stt7-9
C. reinhardtii
NPQ=2.3
B
NPQ
Time since light (sec)
C
Acid
LL
HL
Time (Sec)
stt7-9
C. reinhardtii
+ acetic acid
NPQ=2.2
2 mM KOH
addition

737

Figure 3. Lack of NPQ in *Chlorella ohadii*

(A) Left: Fluorescence traces of dark-adapted LL (top) and HL (bottom) *C. ohadii* grown cells, measured under 2000 µmol photons $m^{-2}s^{-1}$. Up and down arrows indicate the on and off of the actinic light, respectively. Black and yellow colors at the line below the figure indicate dark and actinic light conditions. The red line indicates the time points when saturating pulses were employed to induce maximum fluorescence (F_M and F_M'). Low NPQ was detected as indicated by the little change in F_M' in response to exposure to high light. **Right:** Fluorescence traces of dark-adapted high light grown *stt7-9 C. reinharadtii* cells, exposed to 2000 µmol photons m^{-2} s^{-1}. Note the high NPQ levels.

(B) NPQ values were calculated from the fluorescence traces of dark-adapted LL and HL cells as shown in (A).

(C) NPQ is triggered by high light and acidification of the lumen in *C. reinhardtii* but not in *C. ohadii***. Left:** Fluorescence traces of dark-adapted LL (top) and HL (bottom) *C. ohadii* grown cells, measured under 2000 µmol photons $m^{-2}s^{-1}$ or after the acidification of the media to pH 5.5. Blue arrows indicate turning the light on/off. Black arrows indicate the point of acid addition. **Right:** Fluorescence traces of dark-adapted *stt7-9 C. reinharadtii* cells, exposed to acidic conditions. KOH was added to the cell following 200 sec with no actinic light. The acidification of the medium induced high NPQ levels, mimicking the high light activation of NPQ. This is reversed upon adding KOH, mimicking the light-off action (compare the left panels of **A** and **C**).

Fluorescence was normalized between F_0 and F_M in the dark-adapted cells for all samples.

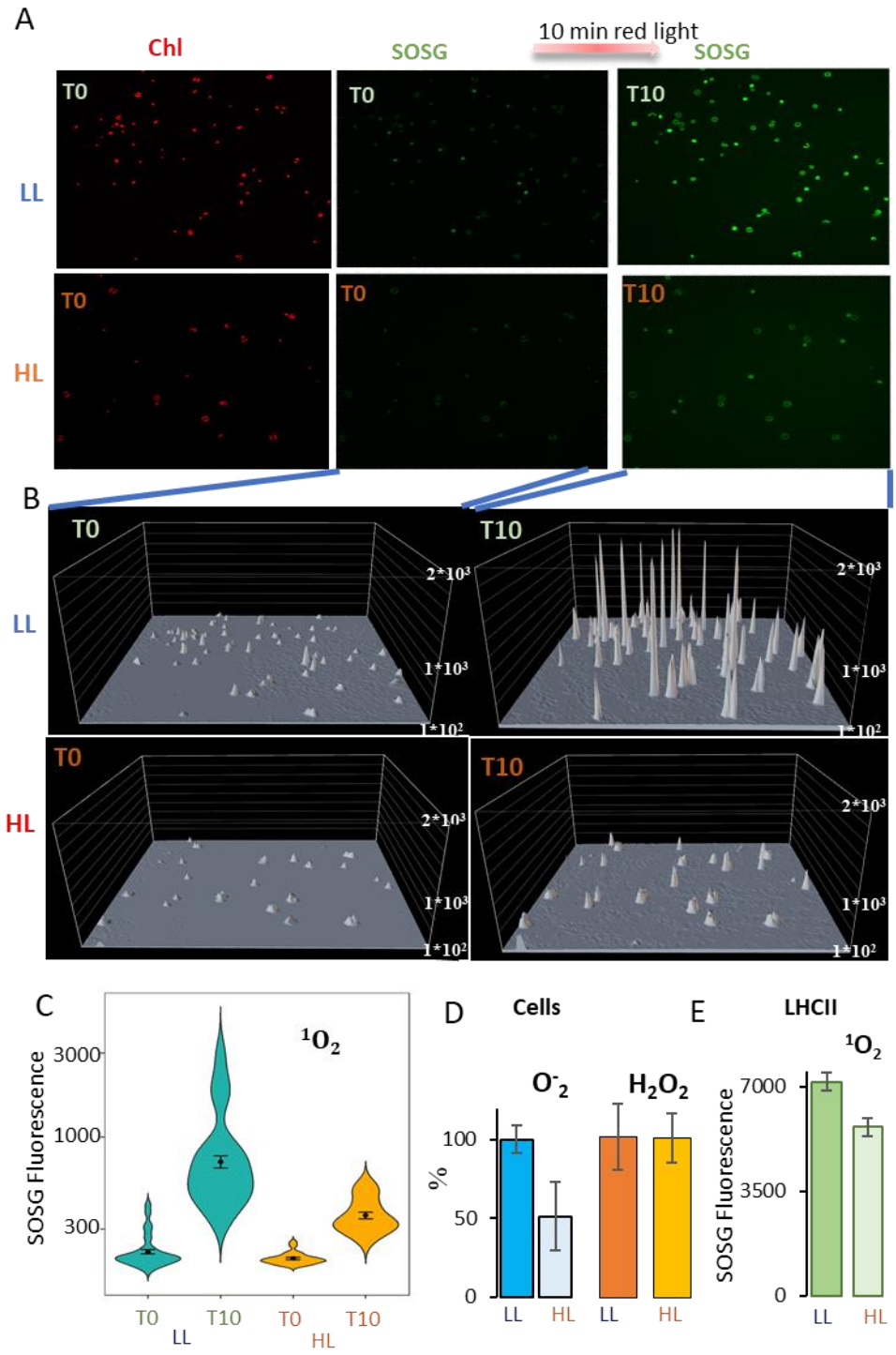
A
Chl
SOSG
10 min red light
SOSG
T0
T0
T10
LL
T0
T0
T10
HL
B
T0
T10
LL
2*10³
1*10³
1*10²
T0
T10
HL
C
SOSG Fluorescence
3000
1000
300
¹O₂
T0
T10
T0
T10
LL
HL
D
Cells
O⁻₂
H₂O₂
%
100
50
0
LL
HL
LL
HL
E
LHCII
¹O₂
SOSG Fluorescence
7000
3500
0
LL
HL

739

Figure 4. HL-grown *Chlorella ohadii* accumulates much less $^1O_2$ than LL-cells.

(A) Confocal microscopy wide-field vision of low and high light (LL and HL)-grown cells. Their intrinsic chlorophyll fluorescent was detected in the left panels to localize the chloroplasts. Note the quenched fluorescence of the HL-grown cells (Levin et al 2021). In the middle and right panels, the fluorescence of the $^1O_2$ marker SOSG is shown, originating from the same chloroplasts that are shown in the left panels. The SOSG fluorescence has been detected before (T0) and after 10 min (T10) of high red-light treatment.

(B) Quantification of $^1O_2$ SOSG signal of the chloroplasts shown in A. Only the SOSG fluorescence that overlaps the intrinsic chlorophyll fluorescent marking the chloroplast has been counted for the quantification (see Supplemented Figure 4).

(C) Violin plots of $^1O_2$ formation following 10 min of illumination with high-intensity red light in 54 and 24 individual chloroplasts of LL and HL-grown cells, respectively. The internal point indicates the mean value and the error bars the standard error (SE). The mean numbers are: LL T0 223, LL T10 723, HL T0 204, HL T10 358. Note the log scale of the y-axis. The statistical analysis was done as described in the methods section.

(D) Accumulation of O^-_2 and H_2O_2 in cells after 10 min of strong light illumination. The formation in HL cells was calculated as a percentage of the formation in LL cells (See methods).

(E) $^1O_2$ accumulation in isolated LHCII complexes after 10 min of strong light treatment was measured by quantifying SOSG fluorescence.

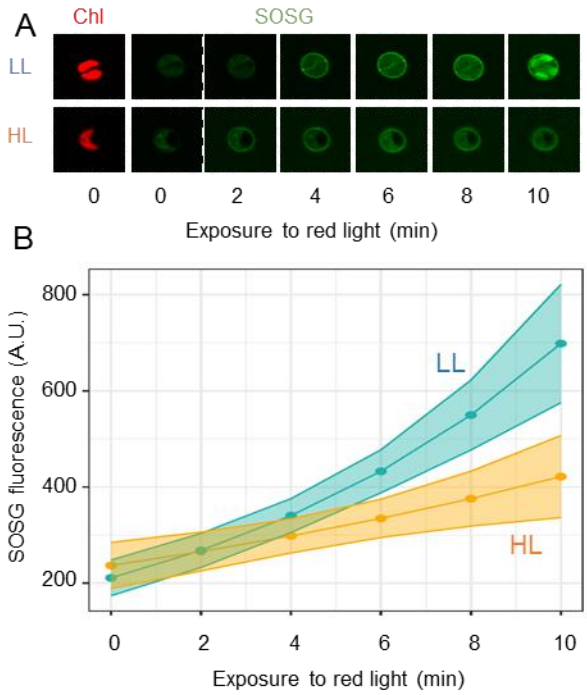

Figure 5. LL-grown *Chlorella ohadii* accumulates significantly more $^1O_2$ within 6 min of exposure to strong light.

(A) Low and high-light (LL and HL)-grown cells were placed in a medium containing the $^1O_2$ marker SOSG in the confocal microscope and chlorophyll fluorescence was detected to locate the chloroplasts in the cells (chl). The cells were then illuminated with strong red light for the times indicated at the bottom and the accumulated $^1O_2$ was detected by the fluorescence intensity of SOSG**.**

(B) Quantification of the SOSG accumulation in 54 and 24 individual chloroplasts from LL and HL-grown cells, respectively, as shown in panel A. Statistical analysis was performed with a linear mixed model of the log10 transformed response with light as fixed effect and time as both fixed and random effect. Shadowed area represents +/- 2*SE. Mixed model ANOVA showed a significant effect of time (p= 0.0027, table x1) and a significant interaction between light and time (p = 3.215E-06, table x1). Post hoc comparisons between treatments in each time point resulted in significant differences in time points 4,6,8,10 (table x2).

A

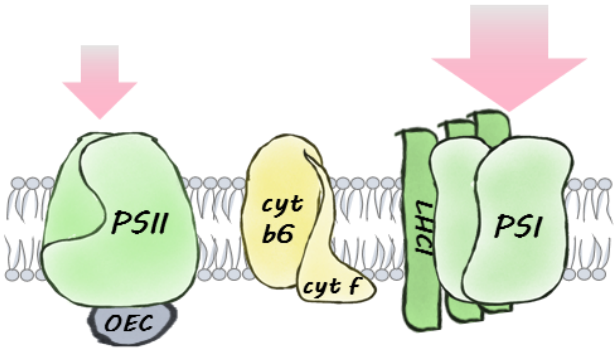

B

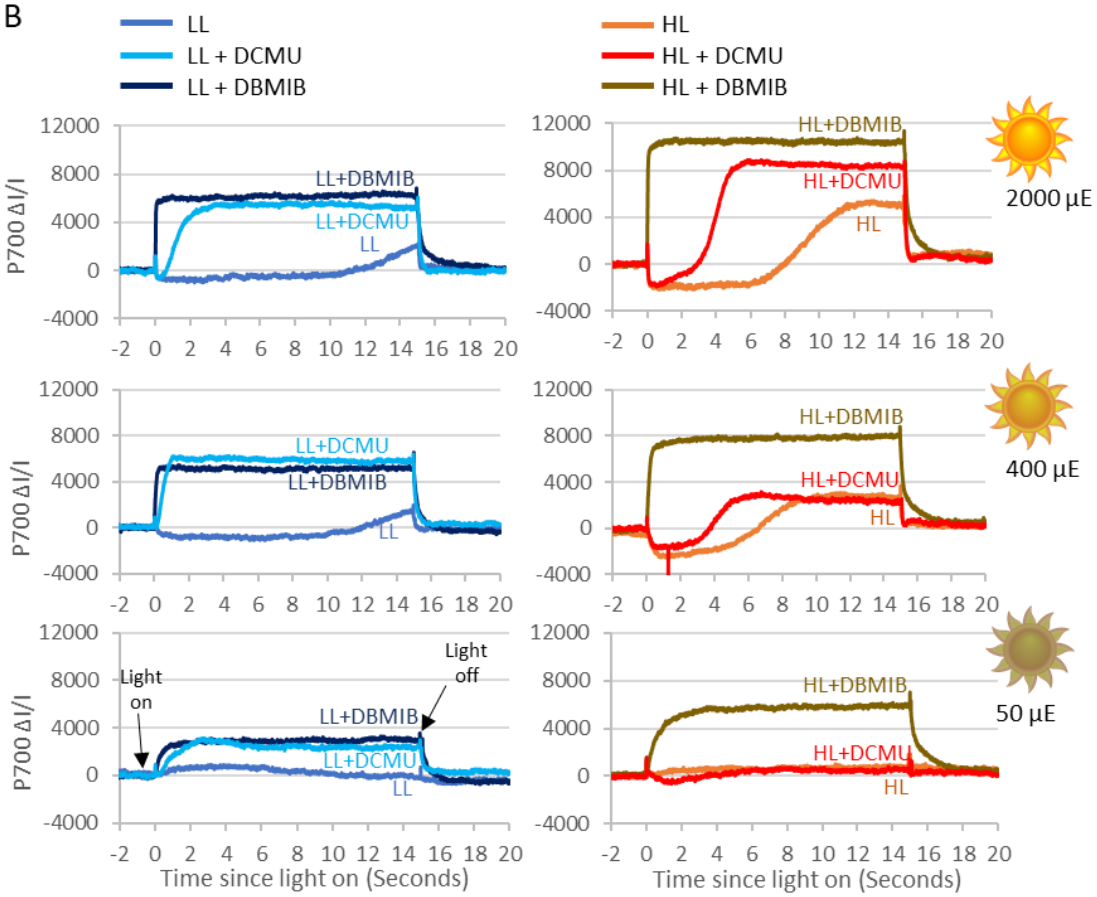

C

Protein	LFQ HL/LL	Protein	LFQ HL/LL
PGR5	1.5	Fd	3.3
PGRL1	1.4	FNR	0.6

759

Figure 6. Cyclic electron flow is highly activated in high-light-grown *C. ohadii*.

(A) In high light (HL)-grown *C. ohadii* the light-harvesting complex II (LHCII) is removed from photosystem II (PSII) while photosystem I (PSI) maintains all or most of its antenna subunits. As a result, PSI is expected to absorb higher quantities of light energy.

(B) P700 oxidation kinetics analysis in dark-adapted cells shows that in the presence of DCMU which blocks linear electron flow (LEF), PSI of HL-grown cells is oxidized at a slower rate compared to that of LL-grown cells in all tested light intensities. When cyclic electron flow (CEF) is blocked by DBMIB, similar PSI oxidation rates are observed in both growth conditions. Note that in LL-grown cells, CEF becomes apparent only by high-light treatment, while in HL-grown cells, CEF is highly activated at all light intensities, and LEF is not activated at very low light intensities. 6 mM methyl viologen was added to all samples.

(C) PGR5, PGRL1, and Fd accumulate in HL-grown cells while FNR accumulates in LL-grown cells, as measured with label-free quantification (LFQ) Liquid chromatography-tandem mass spectrometry (LC-MS/MS).

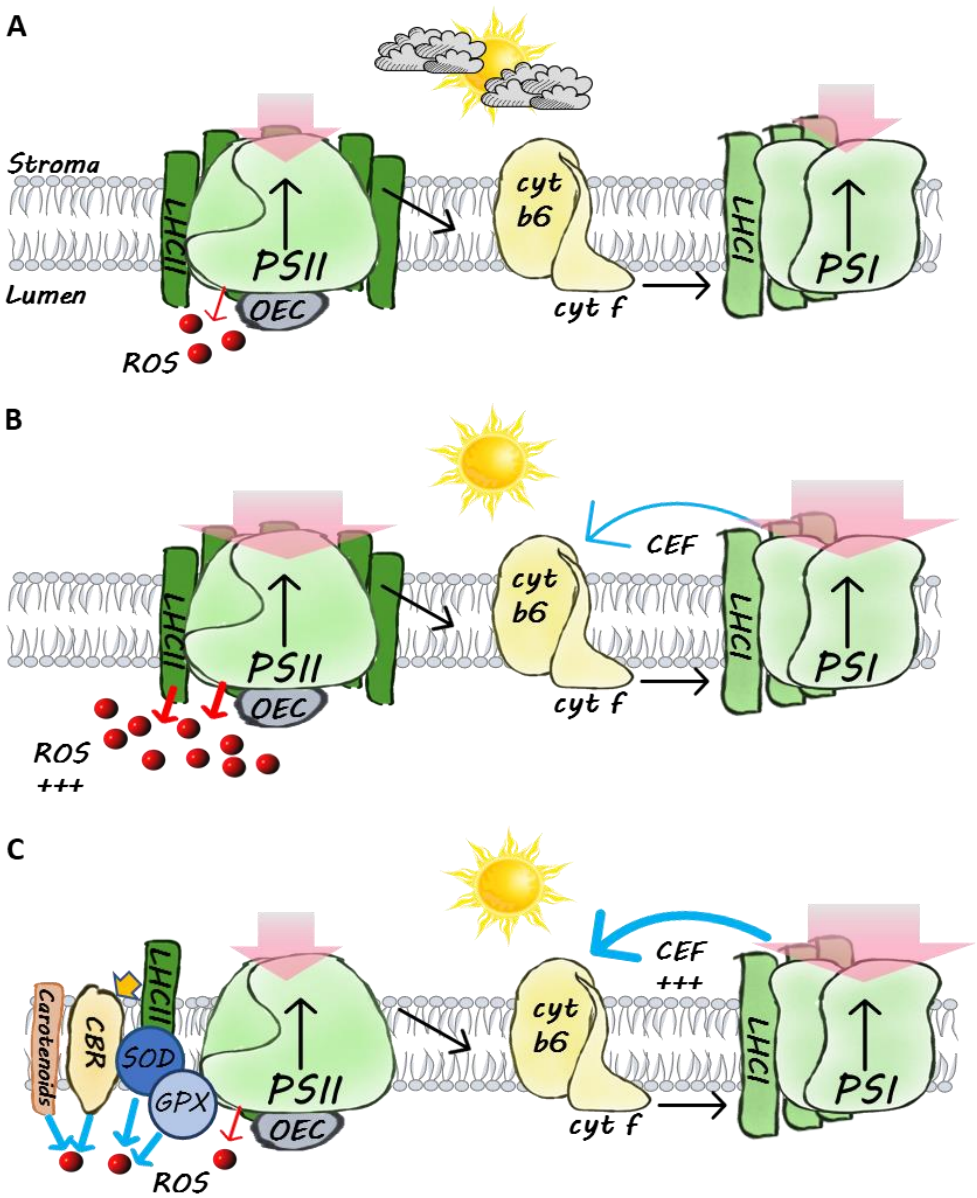
A
Stroma
Lumen
LHCII
PSII
OEC
ROS
cyt b6
cyt f
LHCI
PSI
B
CEF
ROS
+++
C
Carotenoids
CBR
SOD
GPX
CEF
+++

779

Figure 7. *Chlorella ohadii* does not require NPQ for photoprotection.

(A) Under low light (LL) conditions, linear electron flow is favored and small amounts of reactive oxygen species (ROS) are generated.

(B) Upon a shift to high light (HL) conditions, large amounts of ROS are produced by excited chlorophylls in the photosystem II (PSII) and its antenna, as well as the light-harvesting complex II (LHCII). Cyclic electron flow (CEF) around PSI is initiated but is relatively not high.

(C) To avoid light-induced oxidative damage, HL-grown *C. ohadii* eliminates the LHCII, massively reducing the absorption of excess light energy. Additionally, carotenoids, superoxide dismutase (SOD), glutathione peroxidase (GPX), and possibly the carotenoid biosynthesis-related (CBR) protein and other enzymatic antioxidants act as ROS scavengers. CBR may quench light energy that is absorbed by the detached LHCII, before their degradation. CEF is highly activated due to the high levels of absorption in PSI compared to PSII and may provide ATP for metabolic processes.

Supplemental information

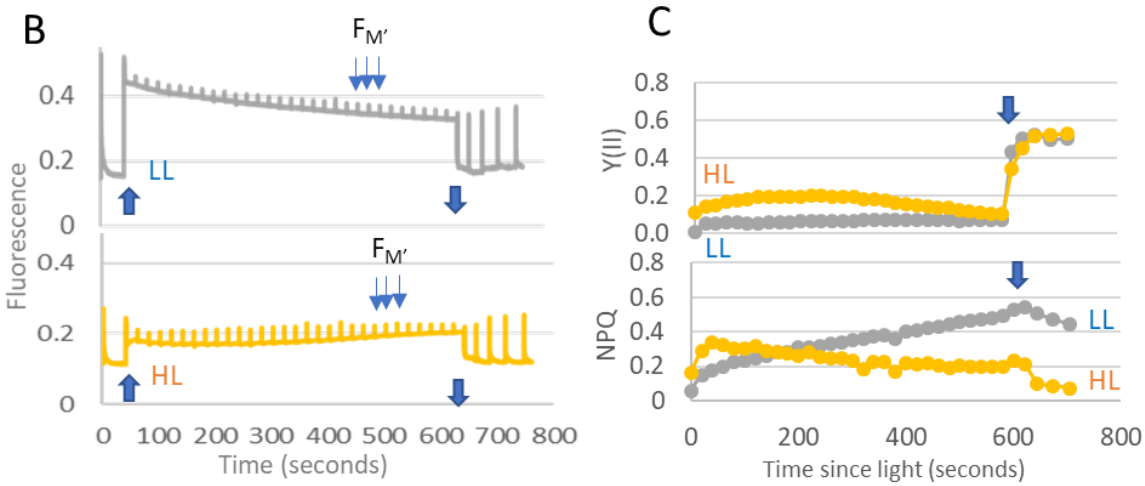

Supplemental Figure 1. *Chlorella ohadii* lacks NPQ under strict photoautotrophic conditions.

(A) Y(II), NPQ, and PSII ETR (ETRII) were calculated from the fluorescence traces of dark-adapted low and high-light (LL and HL) cells grown in mixotrophic conditions, measured under 2000 µmol photons $m^{-2}s^{-1}$ and presented in Figure 3.

(B) Fluorescence traces of dark-adapted LL (top) and HL (bottom) cells grown in strict photoautotrophic conditions, measured under 2000 µmol photons $m^{-2}s^{-1}$. Negligible NPQ was detected as indicated by the little change in maximal fluorescence (F_M) in LL and no change in HL in response to exposure to the pulses of high light.

(C) NPQ and Y(II) values were calculated from fluorescence signals as shown in panel *B*.

LL-grown cells HL-grown cells

3000 µmol photons $m^{-2}s^{-1}$

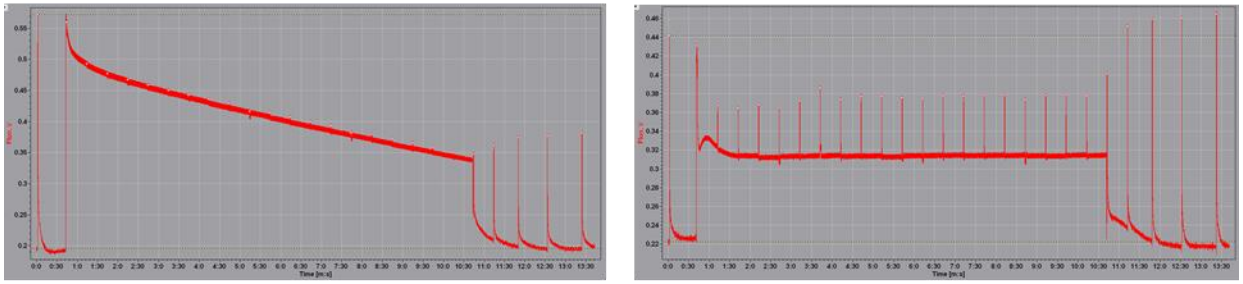

LL 2000 µmol photons $m^{-2}s^{-1}$ HL

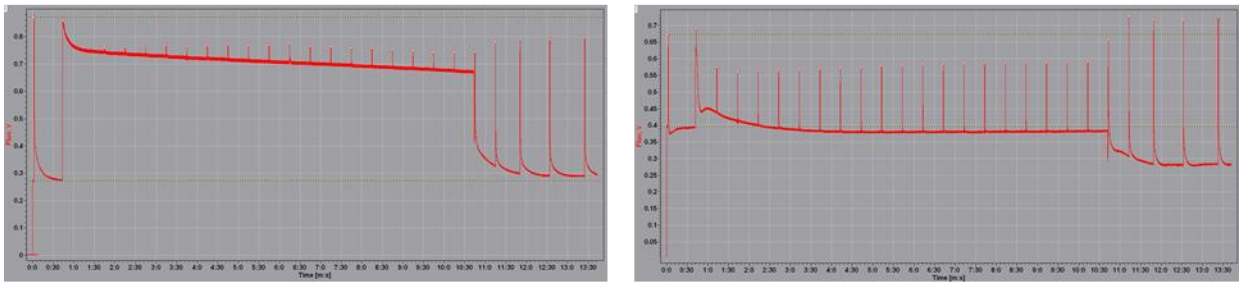

LL 400 µmol photons $m^{-2}s^{-1}$ HL

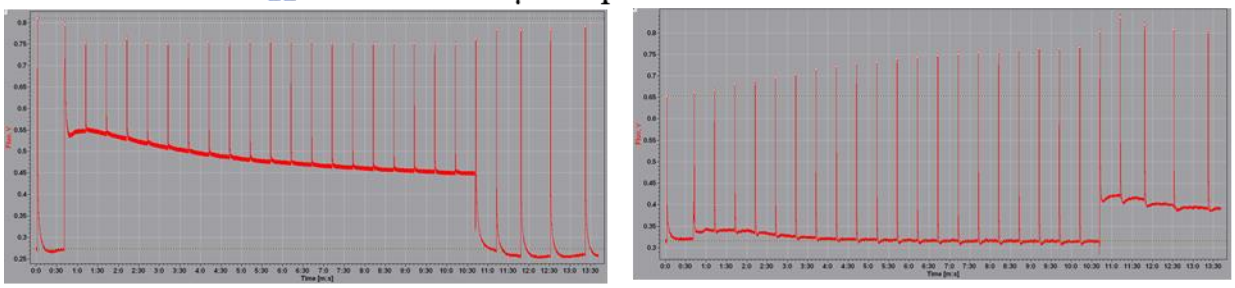

LL 50 µmol photons $m^{-2}s^{-1}$ HL

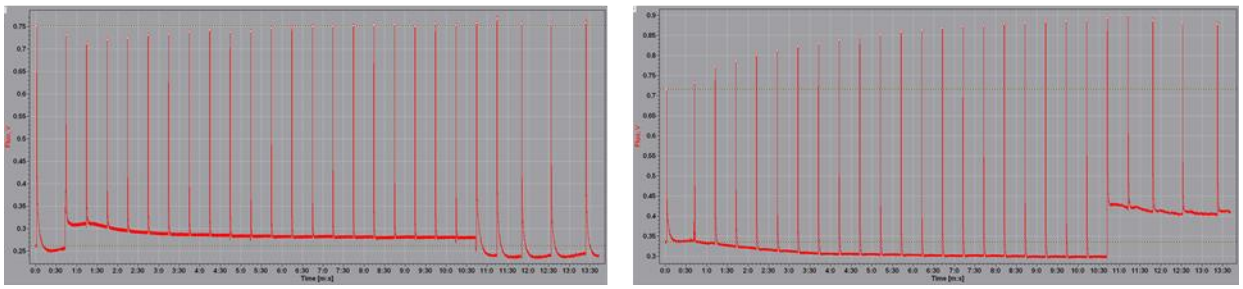

Supplemental Figure 2. *Chlorella ohadii* lacks NPQ under low or high light intensities

Fluorescence traces of dark-adapted low and high light (LL, left, and HL, right)-grown cells. The fluorescence measurement was carried out under different light intensities, as indicated.. Low NPQ was detected as indicated by the little change in F_M' in response to exposure to low or high light.

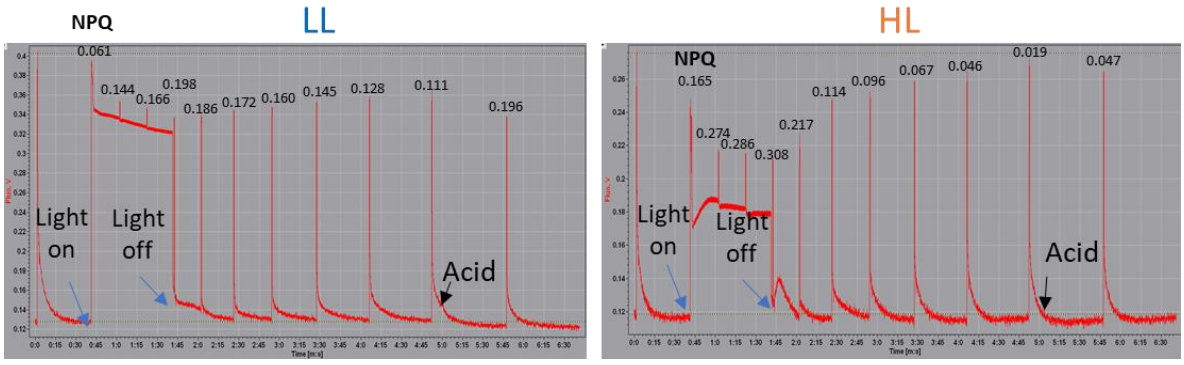

Supplemental Figure 3. NPQ is not induced by high light or acidifying conditions in *Chlorella ohadii* grown under strict photoautotrophic conditions

Fluorescence traces of dark-adapted low and high light (LL, left, and HL, right)-grown cells. First under high light exposure (2000 µmol photons $m^{-2}s^{-1}$), and then quenching was detected in response to the acidification of the media to pH 5.5 with acetic acid. Blue arrows indicate turning the light on/off. Black arrows indicate the point of acid addition. The numbers above each FM signal indicate the NPQ values which are very small compared to *C. reinhardtii* where they are normally 2.2-2.5 (see Figure 3).

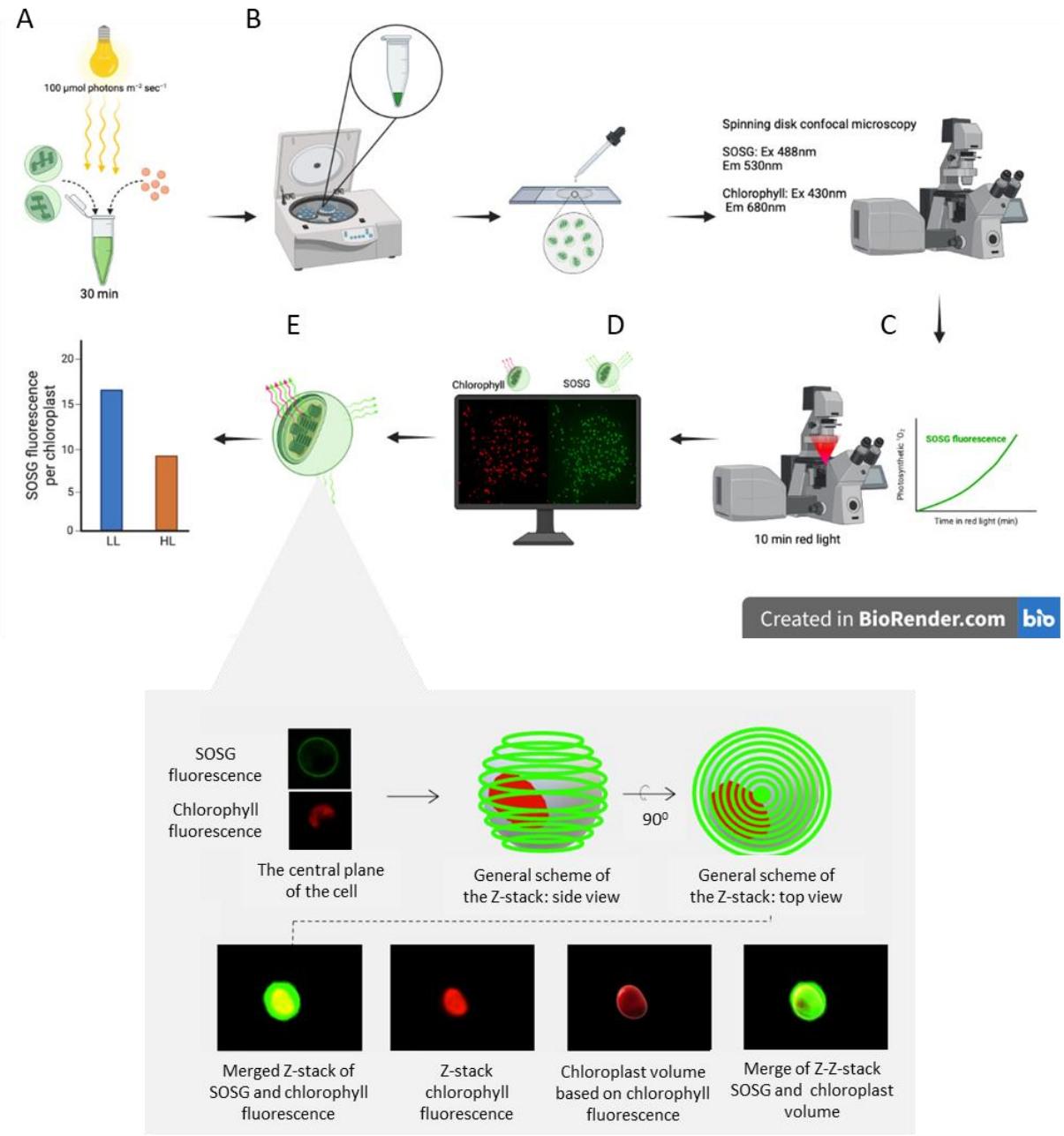
A
B
100 µmol photons m⁻² sec⁻¹
30 min
Spinning disk confocal microscopy
SOSG: Ex 488nm
Em 530nm
Chlorophyll: Ex 430nm
Em 680nm
C
D
E
SOSG fluorescence per chloroplast
20
15
10
5
0
LL
HL
Chlorophyll
SOSG
SOSG fluorescence
Time in red light (min)
10 min red light
Created in BioRender.com bio
SOSG fluorescence
Chlorophyll fluorescence
The central plane of the cell
General scheme of the Z-stack: side view
90⁰
General scheme of the Z-stack: top view
Merged Z-stack of SOSG and chlorophyll fluorescence
Z-stack chlorophyll fluorescence
Chloroplast volume based on chlorophyll fluorescence
Merge of Z-Z-stack SOSG and chloroplast volume

Supplemental Figure 4. $^1O_2$ detection with singlet oxygen sensor green (SOSG) probe work-flow.

(A). SOSG was introduced to LL and HL cells by incubation for 30 min at the light intensity of 100 μmol photons m^{-2} sec^{-1}, with gentle shaking.

(B). The cells were pelleted and resuspended in a fresh TAP medium and loaded onto a microscope slide and applied to a spinning disk confocal microscope with a Z stacking of 8 μm around the cell central plain.

(C). Induction of high light stress was initiated within the microscope using red LED illumination. This wavelength selection (~600 nm) was chosen to specifically activate photosynthesis.

(D). SOSG fluorescence (excitation at 488 nm/emission at 530 nm) was recorded. To locate the chloroplast, chlorophyll fluorescence (excitation at 430 nm/emission at 680 nm) was concurrently recorded.

(E.) Chlorophyll fluorescence was detected in different focused plains before and after the red high light treatment and a 3D model of the fluorescence was created by Z-stacking in the IMARIS program. Due to the limited permeability of SOSG, green fluorescence appeared on the cell membrane throughout the experiments. To subtract the access fluorescence that was not contributed by the photosynthetic-driven $^1O_2$ formation, a chloroplast volume was constructed from the chlorophyll fluorescence.

(F.) SOSG fluorescence was only calculated from the chloroplast volume. This approach ensures the isolation of photosynthetic singlet oxygen formation, offering a comprehensive insight into the dynamics of singlet oxygen accumulation within the cellular context.